Numerical and Experimental Analysis on the Effects of Turbocharged Compressed Bio- Methane Fuelled Automotive Spark-Ignition Engine

Jim Alexander
Vellore Institute of Technology: VIT University
E Porpatham (porpatham.e@vit.ac.in)
Vellore Institute of Technology: VIT University https://orcid.org/0000-0002-4120-8225

Research Article

Keywords: ANSYS, Waste to Energy, Turbocharger, Compressor scroll, Boost pressure, CBM, SI Engine, Performance and Emissions

Posted Date: February 16th, 2021

DOI: https://doi.org/10.21203/rs.3.rs-193776/v1

Version of Record: A version of this preprint was published at Clean Technologies and Environmental Policy on July 18th, 2021. See the published version at https://doi.org/10.1007/s10098-021-02161-5.

Numerical and Experimental Analysis on the Effects of Turbocharged Compressed Bio- Methane Fuelled Automotive Spark-Ignition Engine

Jim Alexander[a], E. Porpatham[a]*

[a] Automotive Research Centre, School of Mechanical Engineering,
Vellore Institute of Technology, Vellore, India
*Corresponding author mail: porpatham.e@vit.ac.in

Abstract

The implementation of recent emission norms has caused the automotive industries to develop advanced technologies for gaseous fuelled SI engines. This research focused on the comparison of turbocharged Compression Ratio (CR) 10.5:1 and naturally aspirated (NA) 12.5:1 for Compressed Bio-Methane (CBM) fuelled SI engine. The original port fuel injected automotive Compressed Natural Gas (CNG) Spark Ignition (SI) engine with 15.5 kW at 3400 rpm was made to function with CBM fuel under full throttle conditions at given CR. Also, two turbochargers T1 and T2 were analysed and validated using ANSYS turbo-machinery numerical package. T1 generated a higher-pressure ratio than T2 and was preferable. The simulation study outcomes infer that entropy generation for T1 at a 1.3 bar is less than 1.5 bar gave a better transient response. The experimental comparison was made between CR of 10.5:1 turbocharged and naturally aspirated CR of 12.5:1. At CR of 10.5:1, 1.3 bar boost pressure, brake power increased by 19.3%, reduced fuel consumption by 10.1%, and reduced hydro carbon (HC) and Carbon monoxide (CO) emissions 42.9% and 38.3%, when compared to NA CR of 12.5:1. On the whole, the downsized CR of 10.5:1 turbocharging exhibit better performance and reduced thermal loading when compared to higher CR of 12.5:1.

Keywords: ANSYS; Waste to Energy; Turbocharger; Compressor scroll; Boost pressure; CBM; SI Engine; Performance and Emissions

Nomenclature

A	Area of the scroll (m^2)
A/F	Air to Fuel ratio
BMEP	Brake Mean Effective Pressure (bar)
BSFC	Brake Specific Fuel Consumption (g/kWh)
CAD	Crank Angle Degree
CBM	Compressed Biomethane
CH_4	Methane
CNG	Compressed Natural Gas
CO	Carbon monoxide
CO_2	Carbon dioxide
COV	Coefficient Of Variation (%)
C_{u2}	Circumferential Velocity at impeller outlet (m/s)
CR	Compression Ratio
EVC	Exhaust Valve Closing
EVO	Exhaust Valve Opening
HC	Hydrocarbon
HP	Horse Power (kW)
h_{t1}	Enthalpy at impeller inlet (kJ/kg)
h_{t2}	Enthalpy at impeller outlet (kJ/kg)
IAT	Intake Absolute Temperature
IMEP	Indicated Mean Effective Pressure (bar)
IMEP	Indicated Mean Effective Pressure (bar)
IVC	Intake Valve Opening
IVO	Intake Valve Closing
k	Ratio of the specific heat capacity
LPG	Liquefied Petroleum Gas
MAP_{req}	Manifold Absolute Pressure required (bar)
N	Engine Speed (rpm)
NA	Naturally Aspirated
NO	Nitric Oxide
NO_x	Oxides of Nitrogen
P_{1c}	Pressure at compressor inlet (kPa)
P_{2c}	Pressure at compressor outlet (kPa)
P_{amb}	Ambient pressure (kPa)
PFI	Port Fuel Injection
r	Centroid radius of the scroll
r_2	Radii at impeller outlet (m)
R_g	Exhaust gas constant (J/kg K)
SI	Spark Ignition
T1	KP31 Turbocharger
T_{1c}	Temperature at compressor inlet (K)

T2	KP35 Turbocharger
T_{2c}	Temperature at compressor outlet (K)
TDC	Top Dead Centre
T_m	Intake Manifold Temperature (K), Rankine to Kelvin scale
V_d	Displacement volume (m^3)
V_e	Volumetric Efficiency
W_a	Air flowrate actual (kg/s)

Greek Symbols

$\dot{m}_T$	Turbine mass flow rate (kg/s)
η_C	Compressor Efficiency
π_c	Pressure ratio
ΔP_{loss}	Pressure losses due to the air filter, intake manifold, and intercooler (kPa)
ω	Turbocharger speed (r/s)

Subscripts

C	Compressor
T	Turbine

1. Introduction

In the developing countries with the higher rural population, there is a requirement towards improving in energy security (Muhumuza et al. 2018), and to reduce greenhouse emissions that affect the climate change (Huppmann et al. 2019), which also meets the UN sustainable development goals (Vu et al. 2015). This has stirred the use of a dedicated source of alternative fuel such as bio-methane for an internal combustion engine. It offers major benefits such as renewable resources, fuel economy and reduced emission levels, compared to conventional fuel, which can also be suitable as transportation fuels more efficiently. The fuel properties are shown in Table 1. This serves as an advantage in utilisation of waste recovery management and the production of cleaner energy. The biomass from anaerobic decomposition generally yields to biogas which has 60% CH4 and 40% CO_2 composition by volume, and it is possible to obtain bio-methane by upgrading the biogas. Different methods can be implemented to upgrade the thermochemical recovery through exhaust gas reformation (Lau et al. 2012), membrane method (Molino et al. 2013), and concurrent elimination (Tippayawong and Thanompongchart 2010) of the contaminants such as CO_2 and H2S is packaged through media column reactors. (Chandra et al. 2011) Compared to the engine's performance operated with biogas under bio-methane, and in comparison, to biogas,

the brake power of the engine operated under bio-methane was increased by approximately 30%. (Bordelanne et al. 2011) A well-to-wheel review to evaluate the potential of natural gas and bio-methane in terms of greenhouse gas emission reductions, and compared the outcomes with gasoline as well. Methane is the primary surrogate of bio-methane neglecting the 2% CO2 and all fossil fuels (Leiker et al. 1972), and its carbon to hydrogen (C/H) ratio is lower. Methane has higher autoignition temperature and reduced flame velocity because the C-H's bond energy is higher than gasoline has renowned anti-knock property (Weaver), (Turns 1996). The engine performance and the combustion cyclic variations, specifically at low loads, are more significant for research. Minimising cyclic variation can be realised by increasing the Compression Ratio (CR). It increases the air to fuel ratio and the mixture density and the turbulence effect of the flame, resulting in higher in-cylinder pressure accompanied by faster flame travel (Costa and Sodré 2011). The cyclic variations result in speed and torque fluctuations which eventually results in vibration of the system.

The investigation and comparison of the performance characteristics of methane with gasoline were done at the wide-open operation of the engine at a different speed. It is also affected by the non-uniformities in air-fuel mixture surrounding the spark plug, and this is characterised by randomness in the motion of the mixture at the vicinity of the spark source during the ignition (Amann 1985). A review of earlier literature states that the experiments conducted in SI engine comparing the performance between methane and gasoline. (Wong 1977) made investigations carried out on the performance characteristics of methane and gasoline at wide-open throttle engine operation for different speed. It was noted that there was a drop in brake power and fuel consumption for methane compared to gasoline. (Arroyo et al. 2013) investigated the features of an SI engine with various fuels and gasoline and methane, at various equivalence ratios and velocities at two throttle positions. It was found that reductions in brake mean effective pressure (BMEP) was observed for methane fuel when compared to gasoline. Whereas the emissions such as HC, CO_2, CO and nitric oxide (NO) exhibited reduced levels for methane fuel compared to gasoline for various engine speed at wide-open throttle and 50% opening. (Thurnheer et al. 2009) subsequently compared combustion characteristics for the engine operation with gasoline and stoichiometric air-fuel methane mixture at 2000 rpm engine speed and 2 bar BMEP. The combustion duration of methane was minimal; however, the duration of combustion was longer than gasoline. A two-zone model was developed by (Pourkhesalian et al. 2010) to simulate the SI engine performance and emission characteristics under various fuels, such as gasoline and methane. They discovered that the engine performance and emission for methane were reduced when

compared to gasoline. Investigations were performed for a direct injection SI engine through an optical version (Serras-Pereira et al. 2013) using different fuels which also included methane, for which the performance, emission and combustion data were obtained and was compared with gasoline fuel in the stoichiometric mode as well as at excess air condition. It was concluded that there was a rise of in-cylinder pressure, and longer combustion duration was observed for methane than gasoline. The influence upon engine performance with methane and natural gas was investigated by (Bommisetty et al. 2018) for a Port Fuel Injection (PFI) SI engine at various speed conditions. Various engine parameters were identified such as in-cylinder pressure, brake thermal efficiency was found and compared to methane, the observations concluded that the Indicated Mean Effective Pressure (IMEP) for methane was reduced, at different loads and speeds compared to natural gas. Comparison of the performance between methane and propane characteristics was investigated by (Moore and Roy 1956). It was concluded that the maximum efficiency by utilisation of propane was greater than that of methane.

Foreseeing from various literature shows that in terms of engine performance and combustion parameters enhancement towards the composition of the biomethane becomes necessary for fuelling the SI engine. Biogas when upgraded results in the formation of compressed biomethane gas (CBM), therefore the composition of biogas upon engine performance must be investigated. To determine engine operational parameters similar to biomethane experimentation, biogas was used as fuel, and engine experimentations were conducted to improvise the engine performance, emission, and combustion characteristics. (Porpatham et al. 2008) found the effect of reduced concentrations of CO_2 in biogas to determine the performance, emissions, and combustion characteristics. It was found that substantial improvement in performance and a reduction in HC emissions when the engine was operated at lower levels of CO_2 composed biogas. It was also noted that at lower CO_2 levels, the lean operation limit was extended. Seeing on the other side the biogas has lower heating value and laminar flame velocity compared to natural gas, and this was due to lower content of CH_4 and the presence of CO_2 (Raju SR 2001), (Chandra et al. 2011), (Cardona and Amell 2013), (Hinton and Stone 2014), leads to lower power output and a reduction in lean operation limit in the engine. Significant research focuses on the biogas composition, which primarily contributes to influencing engine performance. Hence approaches such as adding H2, increasing the CR and turbocharging have proven to maximize the overall engine performance for the biogas fuelled engine. (Porpatham et al. 2007) reported that the biogas with the addition of H2 experimented at different equivalence ratios at a constant speed in a

spark-ignition engine. There was an improvement in brake power and thermal efficiency, and there were also significant reductions in HC emission. (Park et al. 2011) have been studying the effects of adding hydrogen on an engine's behaviour at different excess air ratios and concentrations of CH_4 in biogas. They found that hydrogen addition enhanced the characteristics of in-cylinder combustion, extended the lean limit, and reduced HC emissions. Tests were performed by Porpatham et al. to compare performance, emissions, and combustion characteristics of the engine operated at various CR for a biogas-fuelled spark-ignition. They reported a rise in brake power and thermal efficiency was noted while increasing the CR. They also discovered that when the CR was above a critical value of 13:1, the brake power and brake thermal efficiency increased slightly.

Biogas-fuelled turbocharged engine performance and oxides of nitrogen emissions were studied at different biogas compositions by (Jung et al. 2015). They concluded that the comparison of brake power as a function of boost pressure and relative air/fuel ratio was noted for 50% methane and 50% CO_2 and 70% methane and 30% biogas composition. To obtain a brake power of 22.5 kW, the CH4: CO_2 = 50:50 requires a boosting of 1.14 bar at relative A/F ratio of 1.3 and 1.5 bar at relative A/F of 1.5. The boosting exceeded the range of 1.0-1.5 for the relative A/F ratio of 1.7 and 1.9. For CH4:CO2 = 70:30, the reference brake power attained was 24.8 kW, and the boost pressures were 1.13, 1.27, and 1.44 bar at the relative A/F ratios 1.3, 1.5, and 1.7 respectively. At relative A/F ratio of 1.1, the brake power increases with an increase in boost pressure for both cases denoting the stoichiometric mode. Experiments were conducted for full-load performance with a turbocharged engine. The results concluded that there was a substantial increase in engine torque which was double compared to open wastegate mode fully. There was also an increase in the in-cylinder pressures at turbocharged mode, reduced unburnt HC, and CO emissions (D'Ambrosio et al. 2006) and a better power to weight ratio (Einewall P 1997).

This has led the automotive manufacturer to introduce downsizing concepts that optimize a suitable compression ratio necessary for turbocharging. Recent developments have been made in NA engines for which design parameters at higher compression ratio are brought equivalent to a lower compression engine by means downsizing technique which usually accommodates a turbocharger, this offers enhanced charge cooling, knock free operation, and effective scavenging of the residual gases to improve the low-end torque (Shivapuji and Dasappa 2014), (Padmavathi R, Nandhakumar K 2010). The mass and energy transfer becomes essential parameters that determine a turbocharger's performance, which is necessary for matching. The turbocharger housing unit's design affects the flow rate of air at

the compressor inlet and exhaust backpressure development and flowrate over the turbine. The turbocharger's compressor housing size determines the magnitude of airflow rate, which is required at wide ranges of the engine speed (Mataczynski et al. 2016). The critical element of achieving turbomachine efficiency depends on scroll design. The two main design parameters of the scroll that affect the flow properties are the cross-sectional area (A) and the centroid radius (r) from the rotational centre of the turbo-machinery axis (Niemi SA, Laurén MJ 2002). Selection of the turbocharger required for the engine requires an extensive study of the compressor and a turbine map has to be made with the simulated and experimental results. The turbochargers T1 and T2 are considered for the present study. These turbochargers have radial blade configuration and are usually provided with identical smaller diameters of inducer and exducer for the compressor and turbine. However, the main variations are with the design of the compressor scroll A/r ratio and the volute casing of the exhaust turbine.

To select the right turbocharger, the air flowrate consumption was estimated based on the engine power requirements. Then it was identified on the compressor performance map to determine the range of pressure ratio concerning corrected mass flowrate (for engine experiments actual air flowrate is considered), lines of turbocharger rotational speed, efficiency islands, surge and choke boundaries (Mohan et al. 2019). The flow rate of exhaust gas at the turbine was determined to provide the rotational energy and limit the formation of excessive back pressure using a wastegate actuator. To control the extreme boost pressures, the turbocharger with a wastegate provides the most economical way to improve engine power, torque, and reduce emission (Dobruck et al. 2017). The overall strategy of the literature survey is given in Table 2.

1.1. The novelty of the work

The apparent comparison of CBM fuelled turbocharged SI engine at different boosting at stoichiometric A/F ratio was is not reported. Further, turbocharging the biomethane fuelled engine and its performance, emission and combustion towards minimizing cyclic variation, which altogether reduces the power fluctuations is needed to be carried out. No previous work has been conducted with small version turbocharger selection based on compressor and turbine performance. A direct comparison was done on the engine performance, combustion and emission parameters operating with biomethane fuel. The experiments were conducted at turbocharged CR 10.5:1, and comparisons were made with NA CR 12.5:1. A twin-cylinder,

PFI, liquid-cooled, NA engine was modified to operate with a small-scale turbocharger, having arrangements to vary spark timing and boost pressure.

2. Experimental Setup

Experiments were conducted on a TATA Ace CNG twin-cylinder engine, and a NA converted to turbocharged mode. Also, the CR was varied by varying the thickness of the cylinder head gasket. The engine technical specifications are given in Table 3. The experimental setup layout is shown in Fig. 1. The engine's load was given using the DYNALEC eddy current dynamometer and coupled to a starter motor for motoring or cranking. The engine was modified to a turbocharged version from the NA system suitable for investigating various gaseous fuels. The smaller version turbocharger model was used for turbocharging analysis. An electric wastegate actuator was used to control the exhaust gas's mass flow rate to the turbine. A K-type thermocouple was used to measure the exhaust gas temperature at the exhaust manifold after the turbine outlet. The spark timing was controlled using an in-house developed WOODWARD electronic control unit capable of altering the spark timing. The PFI injectors were replaced by LPG/CNG gas injectors having a working pressure up to 10 bar. The fuel flow rate was determined by FOX thermal mass flowmeter. The airflow rate was determined using an FMG air flowmeter. The intake line consists of an air drum for damping the airflow. An intercooler was placed after the compressor outlet for cooling the high temperature compressed air.

The in-cylinder pressure was measured using KISTLER piezoelectric pressure sensor having a resolution up to 0.1 Crank Angle Degree (CAD). A BOSCH manifold absolute pressure and temperature sensor were mounted before and after the compressor for measuring the intake manifold temperature and pressure. A 0.1 resolution crank angle encoder was coupled to crankshaft and synchronised with a data acquisition system and acquires data for 100 combustion cycles. An oxygen sensor was used to measure equivalence ratio, and the injection system was controlled using a manual feedback loop. The exhaust emissions were measured using a HORIBA five gas analyser which primarily measures the HC, CO, NO and O_2 levels.

The biomethane production was from the fine refinement of the biogas (Serrano JR, Guardiola C, Dolz V, Tiseira A 2007). The biogas was generated in a floating dome reactor where anaerobic digestion of food waste and cow dung takes place. Similarly, the waste source was also obtained from food remains. The gas was collected in a bag and was transported to the laboratory. A separate CO_2 scrubber unit was utilised for upgrading the biogas which separates CO_2 from the biogas composition at desired ranges. Calcium oxide

was mixed with water to obtain calcium hydroxide, this product was filled in the scrubber unit, and the biogas was bubbled through it. The reaction of calcium hydroxide with the CO_2 present in the biogas leads to calcium carbon formation. The scrubbing process done repeatedly till the CO_2 concentrations was attained to the desired levels. The methane and CO_2 concentrations were measured using a non-dispersive infrared analyser. The composition of biogas attained was 84% of methane, 13% of CO_2 and traces of CO and other contaminants. The gas was then taken as a low-pressure inlet from the CO_2 scrubber and fed as the inlet to the high-pressure booster pump, which stores the high-pressure horizontal gas tank's biomethane gas through the multivalve arrangements. The layout of the experimental setup is shown in Fig. 2. The injection pressure was regulated to 2 bar and was delivered to the PFI common rail unit. The measuring instrument's uncertainty was determined by the Gaussian distribution method with an error range of ±2r (Moffat 1988). The accuracy and uncertainty of the instruments used for measurement for experimentation are listed in Table 4.

Initially, experimentations were conducted with NA system at CR 10.5:1 and then turbocharging was performed at 1.1, 1.3 and 1.5 bar boost pressures. Then the experiment was conducted at NA mode at CR 12.5:1. The engine was operated with engine speed at full throttle conditions ranging from 900 rpm to 3400 rpm and fuelled with CBM. The outcome of this research can be realized in commercial vehicles for transportation purpose.

3. Result and Discussion

3.1. Numerical results and analysis of compressor impeller

The research's initial process was carried out in ANSYS Turbomachinery software corresponding to different pressure ratios for T1 and T2 concerning turbocharged engine operating boundary conditions. The compressor parameters were analysed and compared to select the suitable turbocharger. Prediction of the compressor aerodynamic performance for T1 and T2 was initially studied by conducting a steady-state numerical simulation in ANSYS turbomachinery software. The simulation's objective was to evaluate and compare various compressor performance parameters between T1 and T2 at the respective boost pressures. Preliminary calculations were done based on meeting the targeted engine horsepower along with the study conducted upon the compressor variables using the compressor map. The actual mass flow rate of air and pressure ratio was determined from the relations (Garrett

2019) given in equation (1), (2), and (3), considering the non-adiabatic conditions of the turbocharger. In the simulation's initial process, the design details and boundary conditions of the compressor were specified to generate the compressor impeller model.

$$W_a = HP * \left(\frac{A}{F}\right) * \left(\frac{BSFC}{60}\right) \quad (1)$$

$W_a = Air\ Flowrate\ Actual\ (kg/s)$
$HP = Horsepower\ Target\ (kW)$
$A/F = Air\ to\ Fuel\ Ratio$
$BSFC = Brake\ Specific\ Fuel\ Consumption\ (kg/kWh)$

$$MAP_{req} = \left(\frac{W_a * R * (460 + T_m)}{\eta_v * \left(\frac{N}{2}\right) * V_d}\right) \quad (2)$$

$MAP_{req} =$
$Manifold\ Absolute\ Pressure\ (kPa)\ required\ to\ meet\ the\ horsepower\ target$

$W_a = Air\ flowrate\ actual\ (kg/s)$
$R = Gas\ Constant\ (639.6), which\ is\ 287\ J/kgK$
$T_m = Intake\ Manifold\ Temperature\ (K), Rankine\ to\ Kelvin\ scale$
$V_e = Volumetric\ Efficiency$
$N = Engine\ Speed\ (rpm)$
$V_d = Displacement\ Volume\ (m^3)$

$$\pi_c = \frac{p_{2c}}{p_{1c}} = \frac{(MAP_{req} + \Delta p_{loss})}{(p_{amb} - \Delta p_{loss})} \quad (3)$$

$\Pi_c = Pressure\ Ratio$
$p_{2c} = Compressor\ Discharge\ Pressure\ (kPa)$
$p_{1c} = Compressor\ Inlet\ Pressure\ (kPa)$
$MAP_{req} =$
$Manifold\ Absolute\ Pressure\ (kPa)\ required\ to\ meet\ the\ horsepower\ target$

$\Delta p_{loss} =$
$Pressure\ losses\ due\ to\ the\ air\ filter, intake\ manifold\ and\ intercooler\ (kPa)$

$p_{amb} = Ambient\ Pressure\ (kPa)$

The compression work is generally a polytrophic process accompanied by friction and losses in the compressor, which leads to entropy generation. Theoretically, the compressor efficiency is assumed to happen in isentropic conditions that have no heat transfer. However, during the turbocharger's actual engine operating conditions, the compressor is required to

compensate for the losses through additional work. The total-to-total compressor isentropic efficiency was determined (Nguyen-Schäfer 2012) given in equation (4), which denotes the air's energy conversion from the kinetic energy at the impeller to the pressure energy at the diffuser.

$$\eta_c = \frac{\left(\frac{p_{2c}}{p_{1c}}\right)^{\left(\frac{k-1}{k}\right)} - 1}{\left(\frac{T_{2c}}{T_{1c}}\right) - 1} \tag{4}$$

$\eta_c = Compressor\ isentropic\ efficiency$
$p_{2c} = Pressure\ at\ the\ compressor\ outlet\ (kPa)$
$p_{1c} = Pressure\ at\ the\ compressor\ inlet\ (kPa)$
$T_{2c} = Temperature\ at\ the\ compressor\ outlet\ (K)$
$T_{1c} = Temperature\ at\ the\ compressor\ inlet\ (K)$
$k = Ratio\ of\ specific\ heat\ capacity$

The geometric dimensions of the compressor impeller are similar configurations for T1 and T2. The difference is that the compressor scroll is smaller for T1 compared to T2. The specifications of the turbochargers are listed in Table 5. In the pre-processing mode, the overall turbocharger operating ranges and design geometry details were given as input in the Vista CCD, and the compressor impeller model was generated. The overall pressure ratio was 1.5, mass flow 0.03 kg/s, and rotational speed 175000 rpm known from the calibrated values of the compressor maps for T1 and T2. The compressor's inducer and hub diameter are similar for T1 and T2, which are 25 mm and 9 mm respectively, and it has five main radial compressor blades along with splitter blades. The only variations accounted for in the simulation were the air mass flowrate for T1 and T2 based on different engine boost pressures at its corresponding turbocharger speed. Considering the compressor scroll domain, the actual simulation input data were given in terms of analytically calculated inlet air flow rate, which differs individually for T1 and T2, respectively.

From the compressor map the targeted boost pressures necessary for the two-cylinder SI engine, T1 was set to three-speed ranges namely 58%, 80%, and 100% of the overall speed which was expected to attain a maximum pressure ratio up to 1.5. In contrast, for T2, the maximum possible would be 1.1 and speed at 58% of the overall speed. Design points were created from the boundary conditions, and the iteration process was set to simulate the compressor performance. Fig. 3 shows the compressor impeller model generated with the Turbogrid tool's hexahedral mesh, having a total mesh element of 274355.

Fig. 4 and 5, compares the compressor pressure ratio as a function of mass flow rate obtained from the numerical simulation and engine experimentation. The graphical data was superimposed on the original manufacturer compressor maps (Mataczynski et al. 2016) for T1 and T2. The results showed that T1 attained a maximum of 1.5 pressure ratio which has 1.1, 1.3, and 1.5 bar range of boost pressures, whereas T2 attained only 1.1 pressure ratio equivalent to 1.1 bar. At 1.1 pressure ratio, the peak compressor efficiencies were higher for T1 at the lower airflow rate. The higher air flowrate was superior for T2 as shown in This variation in slope between T1 and T2 efficiencies due to flow instabilities and thermal losses. From the comparisons of compressor efficiency shown in Fig. 6, it can be seen that the compressor efficiency reduced for T2 by 16.9% concerning T1, this was due to large stall occurrence which also results in a lesser peak pressure ratio for T2. The factor that affects the compressor efficiency and stability of the flow depends on compressor volute design which varies in size individually for T1 and T2 that significantly influences the axisymmetric flow pattern from the compressor inlet to the diffuser region. T1 has a smaller A/r ratio that accommodates smaller volumes of air and develops a higher-pressure head than T2, which typically has a larger A/r ratio. Therefore, the lower mass flow rate of air T2 scroll has accelerated flow, resulting in reduced total momentum having a final uniform velocity lesser than T1 at the diffuser region. Distortions also influence the additional variations in flow due to bent pipes during real-time engine experimentation.

The numerical results of the blade-to-blade view flow distributions compare the circumferential velocity components between T1 and T2 are shown in Fig. 7. As per the Euler turbine equation (5), since the enthalpy (h_{t2}) of the air medium is higher at the impeller exit results in higher circumferential velocity (C_{u2}) which is higher for T1 compared to T2.

$$h_t = h_{t2} + \omega . r_2 C_{u2} \tag{5}$$

The specific enthalpies (kJ/kg) are denoted by and available at inlet and outlet of the impeller, radii (m) at the impeller outlet, the circumferential velocity of air given as (m/s) at the circumferential direction of the impeller outlet, and is the turbocharger speed is denoted by (r/s). The higher enthalpy causes more work transfer on the air medium by the compressor's impeller blades, leading to the apparent increase in pressure distribution that can be seen from T1 at the impeller exit (Zhao et al. 2020).

The comparison of the compressor impeller's meridional view for T1 and T2 is shown in Fig.8. The static pressure rise at the inducer tip denotes the pressure rise of the impeller. The

pressure rise's main reason was due to higher circumferential velocity at the impeller exit for T1. The other reason is the recirculated flow that tends to lower pressure generation, which is more common in T2, due to the flow rate of air happening in a larger scroll. In contrast, the flow in T2 results in higher pressure development where the compressor scroll matches to engine volume. The compressor efficiency deviation is due to accelerated flow instabilities, flow at sonic velocity, and entropy generation. It is known that the turbocharged engine at lower engine speed has higher levels of residual gas which tends to stall or surge the turbocharger compressor. In the experimental approach at a lower engine speed of 900 rpm, the operating regions for T1 were closer to surge margin within stable limits at all boost pressures. This also had improvements towards low-end engine torque. From the numerical simulation, more significance of surge was observed appearing closer, and beyond the margin, this was due to constant speed input given at each mass flow rate.

At the region of 1.1 pressure ratio, T1 develops higher boost pressure much earlier from lower air flowrate (lower engine speed) and lasts throughout compared to T2. At higher air flowrate (higher engine speed) engine speed regions, the T2 compressor ends up with the choke margin due to the higher generation of volume flow. This was also seen from the actual turbocharged engine experiments with T2. Even at fully closed wastegate conditions, the maximum boost pressure yielded was only 1.1 bar when the engine reached a speed of 3400 rpm. Simultaneously, T1 gave a better transient response and resulted in higher boost pressure development up to 1.5 bar than T2.

The stable operation for T1 was at 1.3 pressure ratio, which was attained at 80% of the turbocharger's overall speed and equivalent to a 140000 rpm speed line. At this operating region, T1 attained having safe surge region at the region of lower air flowrate. It is nearing the efficiency island region and away from the choke region at a higher airflow rate, denoting improvement of higher-pressure ratio. Fig. 6, shows the compressor efficiency as a function of air flow rate at various boost pressure. The compressor efficiency becomes inversely proportional to pressure ratio. The simulation shows that at 1.3 pressure ratio, the compressor efficiency for T1 was 2.9% higher than 1.5. During the compressor compression process, the energy produced per stage causes a rise in temperature with increased pressure. At a higher pressure ratio, the temperature ratio increases; therefore, heat losses occur through the compressor scroll. Overall, it was noted that the scroll design had a significant effect on compressor performance characteristics. This altogether concludes that T1 has better compressor performance than T2 and is suitable for smaller engines.

The Mach number distribution at 1.1, 1.3, and 1.5 bar for T1 are shown in Fig. 9. It is seen that at all boost pressure equivalent pressure ratios, the flow occurs at subsonic ranges less than Mach one. The values tend to be more by 10.8% when the pressure ratio exceeds 1.3, and the flow fields have higher relative velocities at rotational speeds of 175000 rpm. Hence at the higher range of pressure ratio of 1.5, the formation of shock losses tends to be more at the trailing regions of the primary and splitter blades when compared to 1.3. The momentum is comparatively higher with higher rotor speeds due to the higher energy of the rotational stagnation enthalpy during the compression work.

The turbocharger speed ranges 175000 rpm at a higher pressure ratio of 1.5, which causes flow instabilities and causes kinetic energy losses. This causes the compressor efficiency to reduce at a higher-pressure ratio and raises the temperature leading to more compression work to overcome the losses associated with pressure energy. The thermodynamic process of the compressor work can be categorized as an adiabatic and polytropic process. The change in enthalpy between these processes denotes the compressor's additional work towards the attainment of pressure at the output, which compensates for the heat loss due to heat transfer at higher rotor speeds. The contours for entropy at different boost pressure are shown in Fig. 10, for the T1 turbocharger. At a 1.1 pressure ratio at a rotational speed of 101500 rpm, the losses due to flow friction with the blades and heat transfer from the rotor are much lesser. Higher entropy generation occurs at a higher pressure ratio, which is more visible in the primary and splitter blades, and the value becomes 45.8% more for 1.5 pressure ratio compared to 1.3. Thus overall, the conclusions can be drawn from simulation results of compressor performance and blade analysis that for T1 turbocharger was preferable with 1.3 pressure ratio, which is necessary for optimal engine performance.

3.2. On-engine testing of the turbocharger

The performance of T1 and T2 was investigated through on-engine experimentation. The engine experimentations at full throttle conditions were conducted at a naturally aspirated model with PFI of gaseous phase LPG fuel which forms the base readings. The turbocharged engine experiments were then performed by individually testing the turbochargers T1 and T2 to determine its maximum development of boost pressures and corresponding brake power output. The experimental results were compared, which shows the variation of boost pressure with engine speed in Fig 11. The engine speed was operated from 900 rpm to 3400 rpm. The T1 turbocharger started to boost much earlier with a partial closure of the wastegate actuator

than T2. The T1 developed a boost pressure of 1.1 bar which is equivalent to 1.1 pressure ratio at a 25% wastegate actuator position at lower engine speed originating from 1200 rpm engine speed, on the whole, it had superior performance T2.

Further, the boost pressure attained was a maximum of 1.5 bar which was below the knock region. The boost pressure was maintained constant using the wastegate actuator at all engine speed. As a result of the increase in boost pressures, there was higher engine torque and reduced brake specific fuel consumption and emissions. In comparison, T2 had a slower response even at fully closed wastegate conditions towards boost pressure development. It attained a maximum of 1.1 bar at a higher engine speed of 3400 rpm. As mentioned earlier, the smaller A/r ratio of the compressor scroll for the T1 turbocharger resulted in the higher development of pressure ratio than volume flowrate.

For the naturally aspirated engine improvising the intake, airflow becomes an essential factor that denotes the volumetric efficiency (Ve), increasing the BMEP. The variation of Ve as a function of engine speed is shown in Fig. 12. The turbochargers T1 and T2 led a significant increase towards the Ve due to more charged air. At maximum engine torque region and brake, thermal efficiency region of 1800 rpm engine speed the Ve improved for T1 at 1.1, 1.3, and 1.5 bar boost pressures by 10%, 29.3%, and 37.5% and for T2 at 1.1 bar by 4.8% compared to the naturally aspirated model. At lower engine speed regions and 1.1 bar, boosting Ve's values for T1 turbocharger was higher than T2. At higher engine speed T1 has drop-in Ve at 1.1 bar due to inadequate control to regulate the boost pressure exceeding beyond 1.1 bar. This was due to the smaller wastegate hole diameter of the T1 turbine, which results in excessive generation of boosting beyond 1.1 bar. Hence, experimentation venting of air at the intake manifold was done at a higher engine speed to maintain constant boosting. This, however, resulted in higher pumping work due to higher pressure available at the exhaust stroke than the intake. The increase in Ve due to turbocharging has increased the BMEP compared to the naturally aspirated model. The indicated mean effective pressure increases with boosting as a result of better fuel conversion efficiency. The gas work transfer to the piston is not completely transferred, which is available at the driveshaft. The work not utilized is known as the friction work, which also affects the development of boost pressure specifically while turbocharging through all engine factors. The parameter known as the pumping work influences the flow of the working gases at the intake and exhaust manifold. For T1, it becomes necessary to optimize the boost pressures to maximize flow stability. With the engine speed increase towards attaining maximum brake power, the flow becomes choked at the valve seat and reaches the sonic speed. Here it is more significant in the exhaust

manifold of T1 where the pumping work becomes dependent on the exhaust volume, including the port volume, manifold, and turbine volute.

Being a smaller turbine volute for T1, with the increase in boost pressure beyond 1.3 bar it causes an increase in pumping to mean effective pressure and the flow tends to choke when boosting attains 1.5 bar. Among all the boost pressures, 1.5 bar exhibits higher friction values mean effective pressure, signifying the total friction work. The significant losses are pumping work on the fluid medium since the exhaust pressure is relatively higher than the intake. This concludes that T1 having 1.3 bar boost pressure was optimal for overall engine performance.

Overall, the experimental section concludes the necessity to choose T1, and further engine experiments were conducted to determine the engine performance, emission, and combustion parameters.

3.3. Engine performance, emission and combustion parameters

A comparative study and realisation of attaining equivalent performance at turbocharged CR 10.5:1 and NA CR 12.5:1 were analysed for the biomethane fuelled SI engine having composition CH4:CO2=84:13. Various parameters associated with engine performance, emission and combustion were inferred for both conditions.

The Fig. 13, shows the variation of engine torque with speed. The increase in boost pressure leads to increase in engine torque which was more than that of NA at CR 10.5:1 which has a reference engine torque of 42.3 Nm and at boost pressure ss 1.1, 1.3, and 1.5 bar the resultant torque obtained was 47.3, 52.3, 57.3 Nm. The reduction in mechanical and thermal loading at higher CR of 12.5:1 could be minimised through turbocharging at CR 10.5:1. On the other side, it was worth noting that the increase in boosting was limited by knocking. This is also known as abnormal combustion, which drastically rises towards in-cylinder pressure eventually results in knocking. Hence the wastegate must be set to the optimal level of boosting to minimise the mechanical vibrations due to torque fluctuations. Higher boosting the abnormality in combustion leads to unstable combustion, which causes an increase in the Coefficient Of Variation (COV) of Indicated Mean Effective Pressure (IMEP).

The variation of brake power with engine speed is shown in Fig. 14. The effect of increasing the boost pressure resulted in improved brake power which was 35% more at a maximum boosting of 1.5 bar than NA mode for the CR 10.5:1. The intake was admitted more mixture while increasing the boosting, which led to an increase in brake power. The downsizing effect was realized at CR 10.5:1 since the brake power obtained on the onset of turbocharging was

more than or equivalent to NA CR12.5:1. To attain more than the reference brake power of at NA CR 12.5:1 minimum of 1.1 bar boost pressure was necessary. The variation of brake thermal efficiency with speed is shown in Fig. 15. The increase in boost pressure at CR 10.5:1 increased brake thermal efficiency. This is also seen from the otto cycle, where the increase in boost pressure is the same as increasing the CR, hence increasing the boost pressure leads to increased brake thermal efficiency. The variation of brake specific fuel consumption with speed is shown in Fig. 16. The increase in boost pressure led to reduced fuel consumption and was the lowest levels for at 1.5 bar boost. This signifies the maximum energy conversion efficiency through the utilization of fuel energy available as heat energy as BMEP and the exhaust gas recovery through turbocharging altogether leads to lesser fuel consumption for turbocharging at CR 10.5:1.

The variation of HC emission with speed is shown in Fig. 17. There was a significant decrease in HC emission while turbocharging. This can also be attributed to the lower carbon to hydrogen ratio of the biomethane fuel compared to conventional fuel. The maximum reduction in HC emission while boosting at CR 10.5:1 was 50% lower than NA mode, and lower by 46.2% compared to NA CR 12.5:1. Fig. 18, shows the variation of CO emission as a function of engine speed. The effect of boosting led to increased air level in the mixture and, therefore, reduced CO emissions levels, resulting in better oxidation of CO molecules to CO2 during the combustion process. The CO emission lowered by 40% while boosting at CR 10.5:1, this was also at lower levels compared with NA CR 12.5:1. Fig. 19, shows the variation of NO emission as a function of engine speed. The NO levels substantially increased with boosting due to better combustion. However, at 1.5 bar boosting, a finite amount of heat transfer took place due to higher in-cylinder pressure and temperature, which was also from the adiabatic flame temperatures at a 1.3 bar boost. Hence, the NO emission was higher compared to 1.5 bar boosting.

Fig. 20, shows the in-cylinder pressure variations with the combustion cycle number. The in-cylinder pressure analysis gives useful data about the cycle-to-cycle variation for a 100 consecutive combustion cycle number. The in-cylinder pressure was analyzed for the CR 10.5:1 were increasing the boost pressure led to higher levels of in-cylinder pressure. This was also more when compared with NA CR 12.5:1. The higher levels of in-cylinder pressure was due to higher turbulence effects accompanied by faster flame speed. This was also evident from the heat release rate, as shown in Fig. 21, which was higher while the boost pressure was increased. The COV of IMEP shown in Fig. 22, was higher while the boost pressure was increased due to combustion instabilities. At higher boosting and lower engine

speed, the residual gas transfer occurs due to choking of the exhaust gas flow rate, which results in combustion variation and raises the indicated work.

4. Conclusion

In this research work comparison were made among the performance, emission and combustion characteristic by using biomethane fuel for the SI engine operated at full throttle condition maintained at the stoichiometric air-fuel ratio, varying the engine speed from 900 rpm to 3400 rpm for two experimentations, turbocharging at CR 10.5:1 at boost pressures 1.1, 1.3, and 1.5 bar and NA at CR12.5:1 respectively.

- The comparative study reveals that with an increase in boost pressure, the brake power increased by 23.8% compared to NA CR 10.5:1 and 19.3% NA 12.5:1 at an optimal boost pressure of 1.3 bar. There was also an increase in engine torque. This signifies the realization of downsized CR 10.5:1 turbocharging, which attains equivalent engine performance, emission and combustion characteristics when compared with NA CR 12.5:1.
- The increase in boost pressure also increased brake thermal efficiency, and the fuel consumption was also lesser for CR 10.5:1 turbocharging, which was significantly lesser than NA CR 12.5:1.
- The advantage of downsized turbocharging CR 10.5:1 also led to reduced HC, CO and increased levels of NO emission.
- The effect of increasing the boost pressure resulted in increased in-cylinder pressure and heat release rate. This was advisable only to optimal boost pressure since the COV of IMEP was higher at higher boosting of 1.5 bar.

The research conclusions suggest that recently many conventional SI engines within the range of 1L capacity have been in development to adopt gaseous fuelling arrangements viewed from both retrofitted and commercial vehicles. There have been progressive involvements in research to improve their engine performance by introducing alternative fuels that are renewable from bioresources along with the base conventional fuel. Concerning the Ve aspects most necessary for gaseous phase LPG fuelled SI engine, turbocharging has been considered a vital method towards improvement and other gaseous fuels at the downsized range of the engine. The turbocharger can be implemented for small-scaled SI

engines, which has a whole lot of improvement towards engine performance in terms of Ve and brake thermal efficiencies and also reduces HC and CO emission to a greater extent.
Much future work can be developed from the present research, which consists of the multi-fuel gaseous fuelled engine that can accommodate both fuels such as LPG and CBM. Further, the part throttle performance can also be conduct based on the drive cycle test, which is most necessary for meeting the emission standards. Hence turbocharging CNG SI engine can be realized as one of the compact and promising techniques for improving engine performance.

CRediT authorship contribution statement

E. Porpatham: Supervision, Conceptualization, Methodology, Writing- Review, and Editing. **Jim Alexander**: Data Generation, Formal Analysis, Writing- Original Draft, Writing-Review, and Editing.

Conflict of Interests

The authors declare that they have no conflict of interest regarding the publication of this paper.

Acknowledgement

The authors gratefully thank the Science and Engineering Research Board (SERB), India, project No: EMR/2016/004138, for the valuable funding, and Vellore Institute of Technology (VIT), for their immense support to conduct the research work.

References

Amann CA (1985) Cylinder-Pressure Measurement and Its Use in Engine Research. SAE Trans 418–435

Arroyo J, Moreno F, Muñoz M, Monné C (2013) Efficiency and emissions of a spark ignition engine fueled with synthetic gases obtained from catalytic decomposition of biogas. Int J Hydrogen Energy 38:3784–3792. https://doi.org/10.1016/j.ijhydene.2013.01.087

Bommisetty (2018) Fuel Composition Effects in a CI Engine Converted to SI Natural Gas Operation. SAE Technical Paper

Bordelanne O, Montero M, Bravin F, et al (2011) Biomethane CNG hybrid: A reduction by more than 80% of the greenhouse gases emissions compared to gasoline. J Nat Gas Sci Eng 3:617–624. https://doi.org/10.1016/j.jngse.2011.07.007

Cardona CA, Amell AA (2013) Laminar burning velocity and interchangeability analysis of biogas/C 3H8/H2 with normal and oxygen-enriched air. Int J Hydrogen Energy 38:7994–8001. https://doi.org/10.1016/j.ijhydene.2013.04.094

Chandra R, Vijay VK, Subbarao PMV, Khura TK (2011) Performance evaluation of a constant speed IC engine on CNG, methane enriched biogas and biogas. Appl Energy 88:3969–3977. https://doi.org/10.1016/j.apenergy.2011.04.032

Costa RC, Sodré JR (2011) Compression ratio effects on an ethanol/gasoline fuelled engine performance. Appl Therm Eng 31:278–283. https://doi.org/10.1016/j.applthermaleng.2010.09.007

D'Ambrosio S, Spessa E, Vassallo A, et al (2006) Experimental investigation of fuel consumption, exhaust emissions and heat release of a small-displacement turbocharged CNG engine. SAE Tech Pap. https://doi.org/10.4271/2006-01-0049

Dobruck B, Drgo P, Hanko B (2017) Electric servosystem for turbocharger vacuum actuator replacement. Ef Transp 1187–1190

Einewall P JB (1997) Combustion chambers for supercharged natural gas engines. SAE transactions. SAE Trans 408–33

Garrett (2019) Turbo Tech 103 | Expert: Compressor Mapping. 1–13

Gumus M (2011) Effects of volumetric efficiency on the performance and emissions characteristics of a dual fueled (gasoline and LPG) spark ignition engine. Fuel Process Technol 92:1862–1867. https://doi.org/10.1016/j.fuproc.2011.05.001

Hinton N, Stone R (2014) Laminar burning velocity measurements of methane and carbon dioxide mixtures (biogas) over wide ranging temperatures and pressures. Fuel 116:743–750. https://doi.org/10.1016/j.fuel.2013.08.069

Huppmann D (2019) IAMC 1.5°C Scenario Explorer and Data hosted by IIASA.

Jung C, Park J, Song S (2015) Performance and NOx emissions of a biogas-fueled turbocharged internal combustion engine. Energy 86:186–195. https://doi.org/10.1016/j.energy.2015.03.122

Koonaphapdeelert S, Aggarangsi P, Moran J Biomethane

Lau CS, Allen D, Tsolakis A, et al (2012) Biogas upgrade to syngas through thermochemical recovery using exhaust gas reforming. Biomass and Bioenergy 40:86–95. https://doi.org/10.1016/j.biombioe.2012.02.004

Leiker M (1972) Evaluation of Antiknocking Property of Gaseous Fuels by Means of Methane Number and Its Practical Application to Gas Engines. 345 E 47TH ST, NEW YORK, NY 10017: ASME-AMER SOC MECHANICAL ENG

Mataczynski MR, Litke P, Naguy B, Baranski J (2016) Characterization of Small-Scale Turbochargers for Unmanned Aerial Systems. SAE Tech Pap 2016-Novem: https://doi.org/10.4271/2016-32-0078

Moffat RJ (1988) Describing the uncertainties in experimental results. Exp Therm Fluid Sci 1:3–17. https://doi.org/10.1016/0894-1777(88)90043-X

Mohan A, Jaliwala J, Bhagat K, Patchappalam K (2019) A Comprehensive Study on Euro 6 Turbocharger Selections and Its Deterioration with Closed Crank-Case Ventilation in Heavy Commercial Vehicles. SAE Tech Pap 2019-Septe: https://doi.org/10.4271/2019-24-0061

Molino A, Migliori M, Ding Y, et al (2013) Biogas upgrading via membrane process: Modelling of pilot plant scale and the end uses for the grid injection. Fuel 107:585–592. https://doi.org/10.1016/j.fuel.2012.10.058

Moore NPW, Roy BN (1956) Comparative Studies of Methane and Propane as Engine Fuels. Proc Inst Mech Eng 170:1157–1172. https://doi.org/10.1243/pime_proc_1956_170_095_02

Muhumuza R, Zacharopoulos A, Mondol JD, et al (2018) Energy consumption levels and technical approaches for supporting development of alternative energy technologies for rural sectors of developing countries. Renew Sustain Energy Rev 97:90–102. https://doi.org/10.1016/j.rser.2018.08.021

Nguyen-Schäfer H (2012) Efficiencies of Compressor and Turbine. Rotordynamics Automot turbochargers 18–20. https://doi.org/10.1007/978-3-319-17644-4

Niemi SA, Laurén MJ MT (2002) Effect of waste-gate turbocharging on the exhaust particulate matter of an off-road diesel engine. SAE Tech Pap

Padmavathi R, Nandhakumar K DP (2010) Effect of turbocharging geometrical configurations on engine performance and emissions. In: Proc. 10th Int. Symp., Stuttgart. Stuttgart, Germany

Park C, Park S, Lee Y, et al (2011) Performance and emission characteristics of a SI engine fueled by low calorific biogas blended with hydrogen. Int J Hydrogen Energy 36:10080–10088. https://doi.org/10.1016/j.ijhydene.2011.05.018

Porpatham E, Ramesh A, Nagalingam B (2008) Investigation on the effect of concentration of methane in biogas when used as a fuel for a spark ignition engine. Fuel 87:1651–1659. https://doi.org/10.1016/j.fuel.2007.08.014

Porpatham E, Ramesh A, Nagalingam B (2007) Effect of hydrogen addition on the performance of a biogas fuelled spark ignition engine. Int J Hydrogen Energy 32:2057–

2065. https://doi.org/10.1016/j.ijhydene.2006.09.001

Porpatham E, Ramesh A, Nagalingam B (2013) Effect of swirl on the performance and combustion of a biogas fuelled spark ignition engine. Energy Convers Manag 76:463–471. https://doi.org/10.1016/j.enconman.2013.07.071

Pourkhesalian AM, Shamekhi AH, Salimi F (2010) Alternative fuel and gasoline in an SI engine: A comparative study of performance and emissions characteristics. Fuel 89:1056–1063. https://doi.org/10.1016/j.fuel.2009.11.025

Qi DH, Lee CF, Safety A (2014) International Journal of Sustainable Combustion and emissions behaviour for ethanol – gasoline-blended fuels in a multipoint electronic fuel injection engine. 37–41. https://doi.org/10.1080/14786451.2014.895004

Raju SR (2001) Experimental investigation on the performance of a lean burn spark ignition gas engine [Ph. D Thesis]. IIT Madras

Serrano JR, Guardiola C, Dolz V, Tiseira A CC (2007) Experimental study of the turbine inlet gas temperature influence on turbocharger performance. SAE Tech Pap

Serras-Pereira J, Aleiferis PG, Richardson D (2013) An analysis of the combustion behavior of ethanol, butanol, iso-octane, gasoline, and methane in a direct-injection spark-ignition research engine. Combust Sci Technol 185:484–513. https://doi.org/10.1080/00102202.2012.728650

Shivapuji AM, Dasappa S (2014) Selection and thermodynamic analysis of a turbocharger for a producer gas-fuelled multi-cylinder engine. Proc Inst Mech Eng Part A J Power Energy 228:340–356. https://doi.org/10.1177/0957650913517677

Thurnheer T, Soltic P, Dimopoulos Eggenschwiler P (2009) S.I. engine fuelled with gasoline, methane and methane/hydrogen blends: Heat release and loss analysis. Int J Hydrogen Energy 34:2494–2503. https://doi.org/10.1016/j.ijhydene.2008.12.048

Tippayawong N, Thanompongchart P (2010) Biogas quality upgrade by simultaneous removal of CO2 and H2S in a packed column reactor. Energy 35:4531–4535. https://doi.org/10.1016/j.energy.2010.04.014

Turns SR (1996) Introduction to combustion. McGraw-Hill Companies

Vu TKV, Vu DQ, Jensen LS, et al (2015) Life cycle assessment of biogas production in small-scale household digesters in Vietnam. Asian-Australasian J Anim Sci 28:716–729. https://doi.org/10.5713/ajas.14.0683

Weaver CS Natural Gas Vehicles — A Review of the State of the Art

Wong JK (1977) Study of mixtures of methane and carbon dioxide as fuels in a single cylinder engine (CLR). SAE Tech Pap

Zhao B, Zhao Q, Zhao W, et al (2020) Numerical and experimental investigation of turbocharger compressor low-end performance improvement using a variable geometry inlet orifice. Int J Engine Res. https://doi.org/10.1177/1468087420951097

List of Tables

Table 1

Properties of the fuels (Gumus 2011), (Qi et al. 2014), (Porpatham et al. 2013), (Koonaphapdeelert et al.)

Properties	Gasoline	LPG	CNG	CBM
Chemical Structure, Composition (% vol)	C_4 to C_{12}	$C_3H_8 + C_4H_{10}$ Propane C_3H_8 – 30% Butane C_4H_{10} – 70%	CH_4 – 85% C_2H_6 – 7% C_3H_8 – 2% N_2 – 1% CO_2 – 5%	CH_4 – 84% CO_2 – 13%
	42.8	45.7	50	33.7
Lower heating value (MJ/kg)	0.742	2.26	0.79	0.9
Density (kg/m^3)	33	38.25	34	-
Flame velocity (cm/s)	14.7	15.5	17.3	12.64
Stoichiometric Air Fuel Ratio (kg/kg)	0.6 – 8	2.15 – 9.6	5 – 15	-
Flammability limits (vol.% in air)	90	103 – 105	120	-
Research octane number	81 – 89	90 – 97	120	-
Motor octane number	~300	405 – 450	540	-
Auto ignition temperature (^{o}C)				

Table 2. Noteworthy Literature studies on turbocharging of CBM fuelled SI engine

Investigators	Turbocharged SI engine with CBM fuelled operating conditions	Inference
D'Ambrosio et al. 2006	Experiments were performed for full-load performance with an SI engine	There was a strong rise in engine torque. Consequently, there was an increase in the in-cylinder pressure, reduction in HC and CO emission
Einewall P 1997	Incorporating gaseous fuelled SI engine such as CNG vehicles with turbocharger results in better power to weight ratio	Increasing the air in the intake mixture causes the volumetric efficiency to increase, which in turn improves the engine horsepower
Chandra et al. 2011	The engine performance was investigated between biomethane and biogas fuel	Biomethane gave 30% improvement in compared to biogas
Amann 1985	The engine performance investigation and were made between methane and gasoline fuel at the wide-open operation	The results concluded that instabilities in ai-fuel mixture occurs at the vicinity of the spark plug
Jung et al. 2015	Biogas-fuelled turbocharged engine performance was investigated at different biogas compositions	The effect of boost pressure improved the brake power at different equivalence ratio

Table 3
Engine specifications.

Type	Four stroke, liquid cooled, twin cylinder, overhead valve, SI engine
Make	TATA Ace CNG
Fuel	Compressed Biomethane (CBM)
Number of cylinders	Two
Bore x stroke	75 x 79.5 mm
Displacement volume	702 cc
Compression ratio	10.5:1 and 12.5:1
Connecting rod length	142 mm
Rated power	15.5 kW @ 3400 rpm
Valve timing	Cylinder 1 Inlet valve opening: 17^{o} before TDC Inlet valve closing: 235^{o} after TDC

	Exhaust valve opening: 210° before TDC Exhaust valve closing: 17° after TDC Cylinder 2 Inlet valve opening: 20° before TDC Inlet valve closing: 234° after TDC Exhaust valve opening: 177° before TDC Exhaust valve closing: 15° after TDC

Table 4

List of instruments used and its accuracy and uncertainty.

S.No	Measuring Instruments	Make	Accuracy	Uncertainty
1	Airflow meter	FMG Series Rotary Gas Meter	±2% full scale reading	-
2	Fuel flow meter	Fox Thermal Model FT3 Thermal Gas Mass Flowmeter	±0.2% of full scale reading	-
3	Pressure pick up Piezo-electric	KISTLER, Switzerland	±0.5% full scale reading	0.846
4	Combustion Analyser	KISTLER KiBox To Go Type 2893A	-	-
5	Crank Angle Adapter	KISTLER Type 2619A11	0.1 deg CA	Approx. 5 ms (<< 1 combustion cycle)
6	IAT Sensor	VW AG	-	-
7	MAP and IAT Sensor	Bosch	-	-
8	Five gas analyzer	HORIBA, Japan	CO: ± 0.07% of full scale reading CO_2: ± 0.53% of full scale reading	±3.92% ±3.92%
9	Dynamometer	DYNALEC, India HBM, India	Speed: ±0.5% of full-scale reading Load: ±0.25% of full-scale reading	±2 ±0.5

Table 5

Specifications of the turbocharger T1 and T2.

Specifications	T1	T2
Compressor Inducer Diameter (mm)	25	25
Compressor Exducer Diameter (mm)	37	37
Turbine Exducer Diameter (mm)	35	35
Turbine Inducer Diameter (mm)	27	27
Compressor Scroll A/r ratio	Smaller	Larger
Rotor Speed (rpm)	240000	300000
Pressure Ratio	2.2	3
Corrected Air flowrate (lb/min)	8	10
Compressor Housing Material	Aluminium	Aluminium
Turbine Housing Material	Cast Iron	Cast Iron
Cooling System	Oil Cooled	Oil Cooled
Wastegate actuator	Electric	Electric

List of Figures

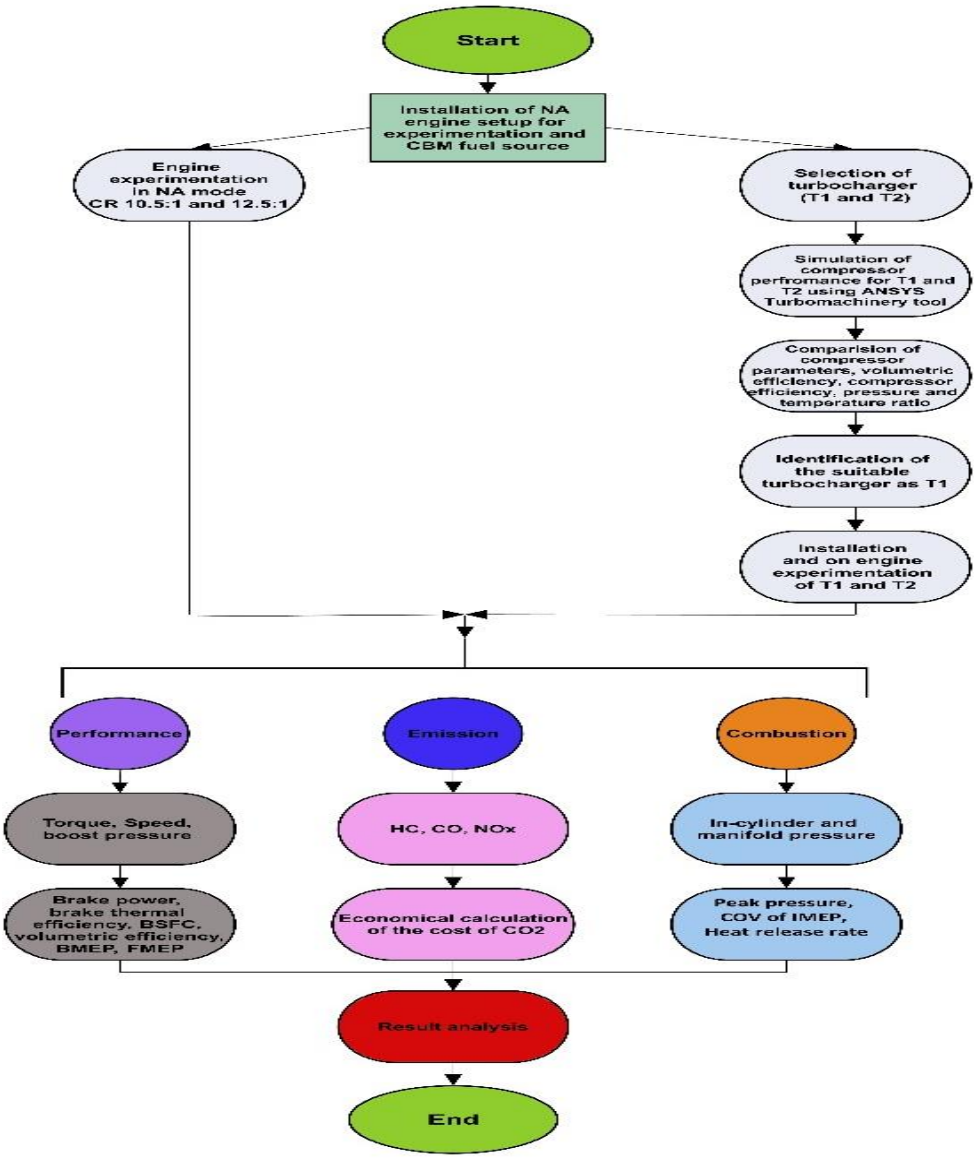

Fig. 1. Test plan for simulation and experimental procedures

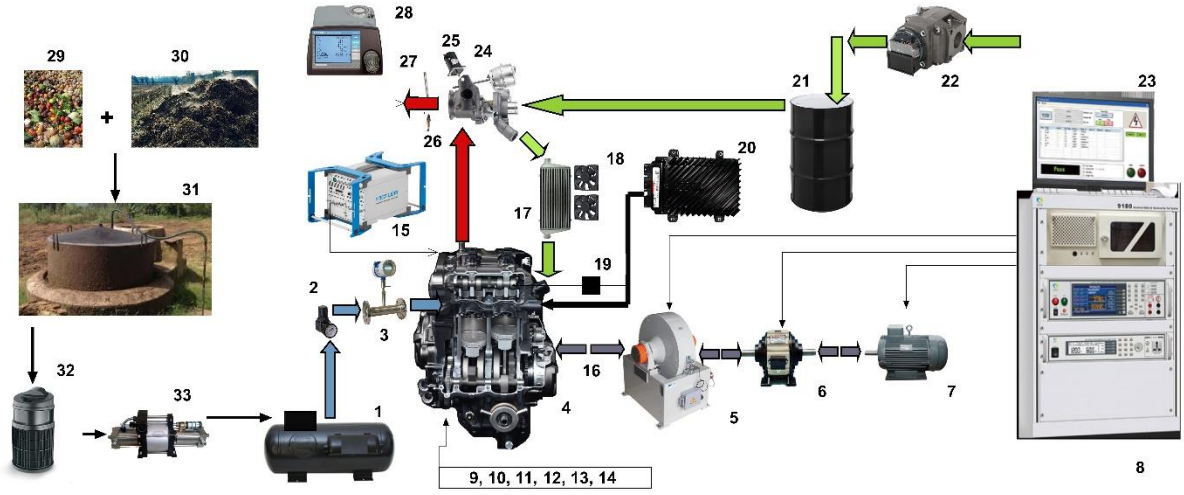

1. Gas Tank with multivalve - Compressed Biomethane (CBM) 2. Pressure regulator 3. Fuel flowmeter 4. Engine 5. Eddy current dynamometer
6. Electromagnetic clutch 7. Motor 8. Dynamometer controller 9. Cam sensor 10. Crank sensor 11. Spark plug
12. Port fuel injector 13. In-cylinder pressure sensor 14. IAT and MAP sensor 15. Combustion analyser 16. Universal joint
17. Intercooler 18. Cooling fan 19. Ignition coil 20. Engine control unit 21. Air drum 22. Air flowmeter 23. User interface
24. Turbocharger 25. Electric wastegate actuator 26. Oxygen sensor 27. Exhaust gas temperature sensor 28. Emission analyser
29. Food waste 30. Cow dung 31. Floating drum - anaerobic digester 32. CO2 scrubber 33. High pressure booster pump

Fig. 2. Schematic layout of the experimental setup.

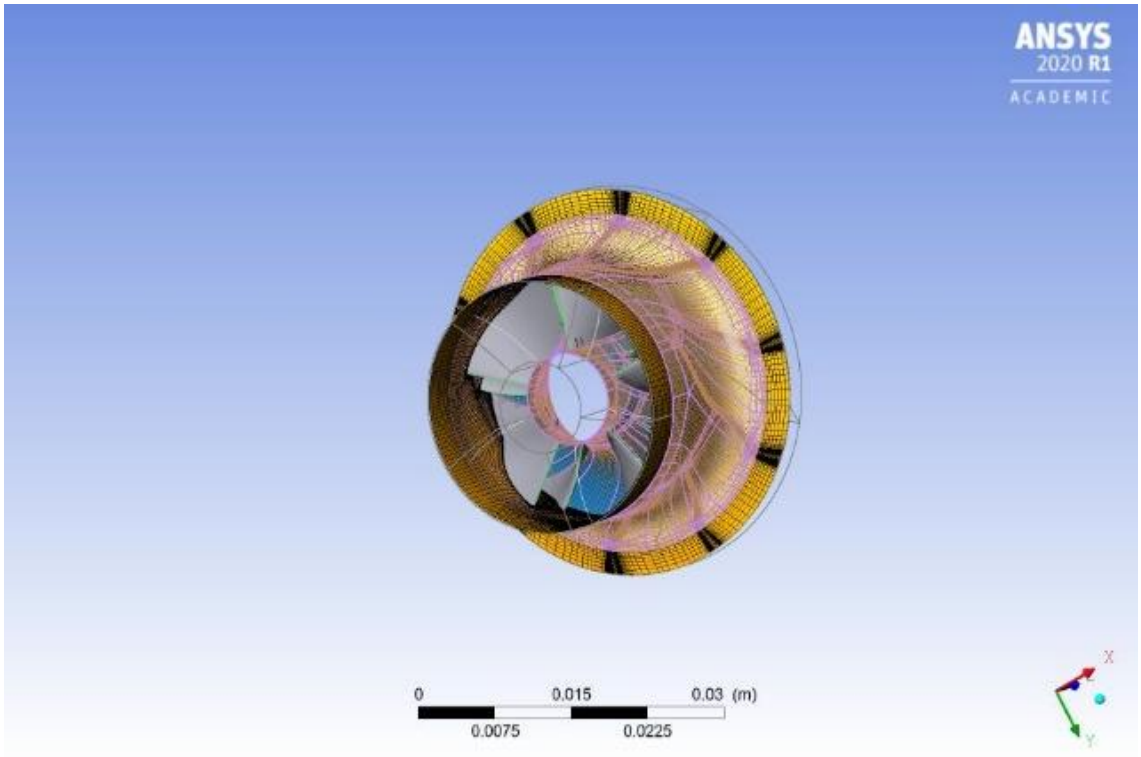

Fig. 3. Meshed view of the compressor impeller.

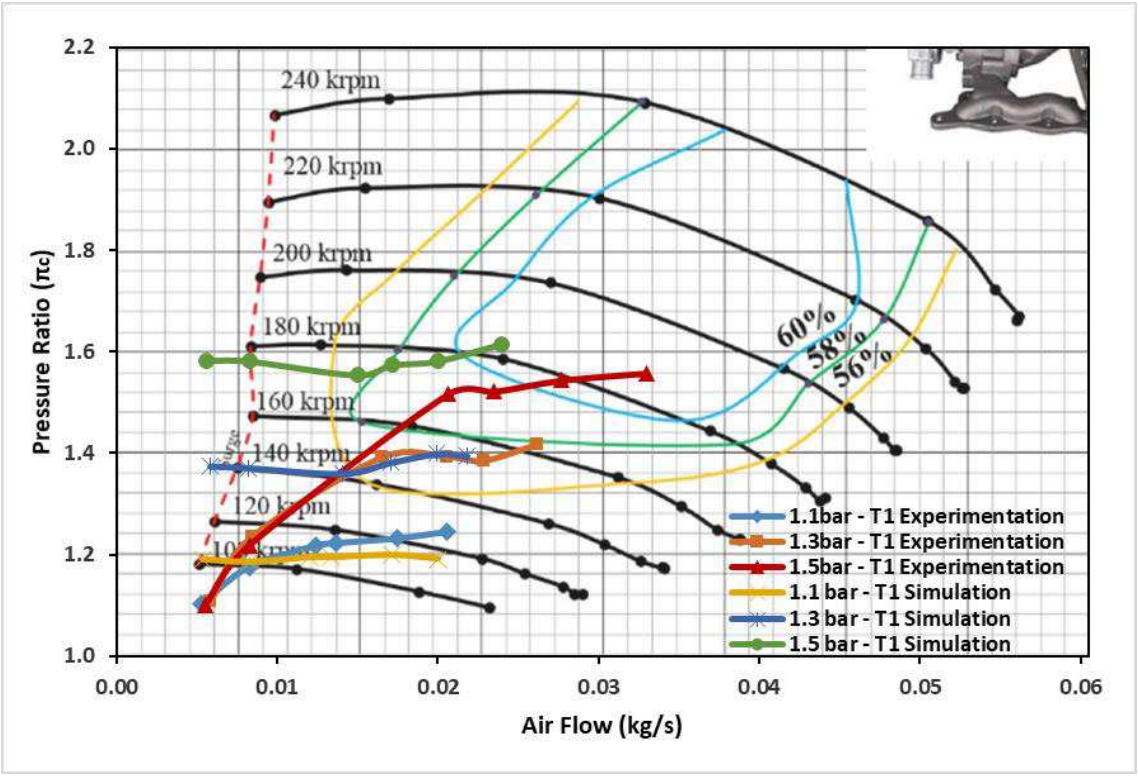

Fig. 4. Variation of pressure ratio with airflow for T1.

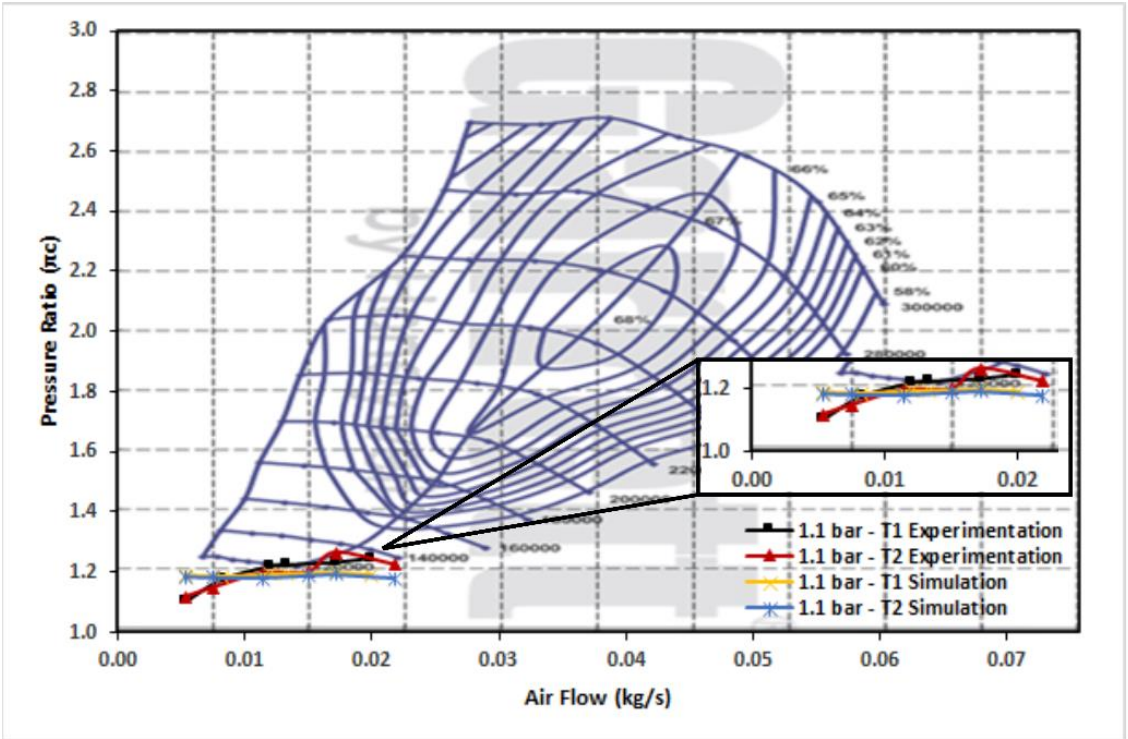

Fig. 5. Variation of pressure ratio with airflow for T2.

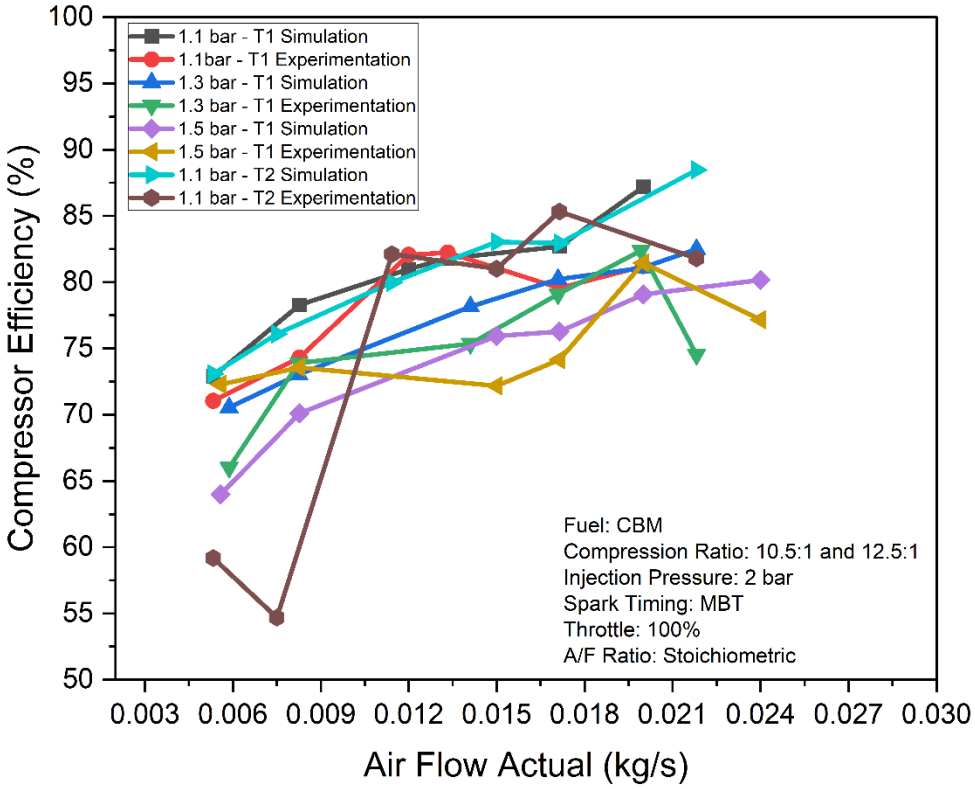

Fig. 6. Variation of compressor efficiency with airflow for T1.

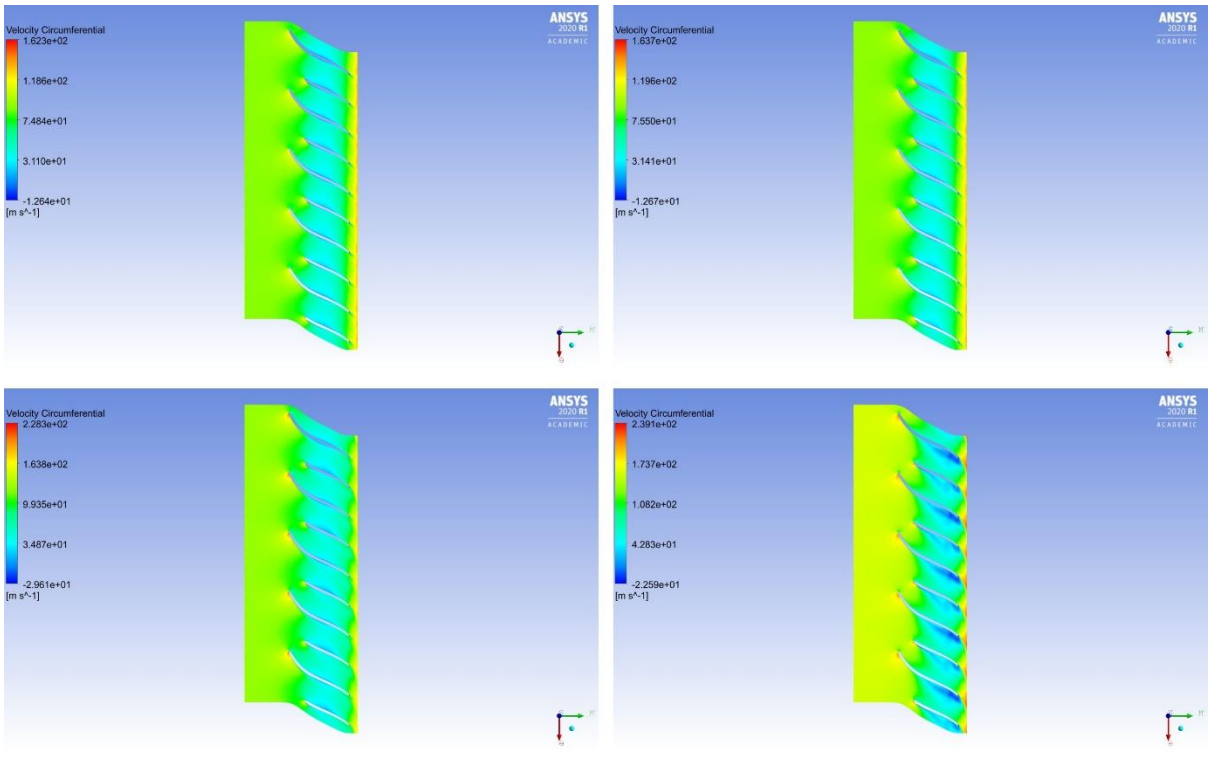

Fig. 7. Blade to blade view circumferential velocity distribution for

T2 1.1 pressure ratio and T1 1.1, 1.3, 1.5 pressure ratio.

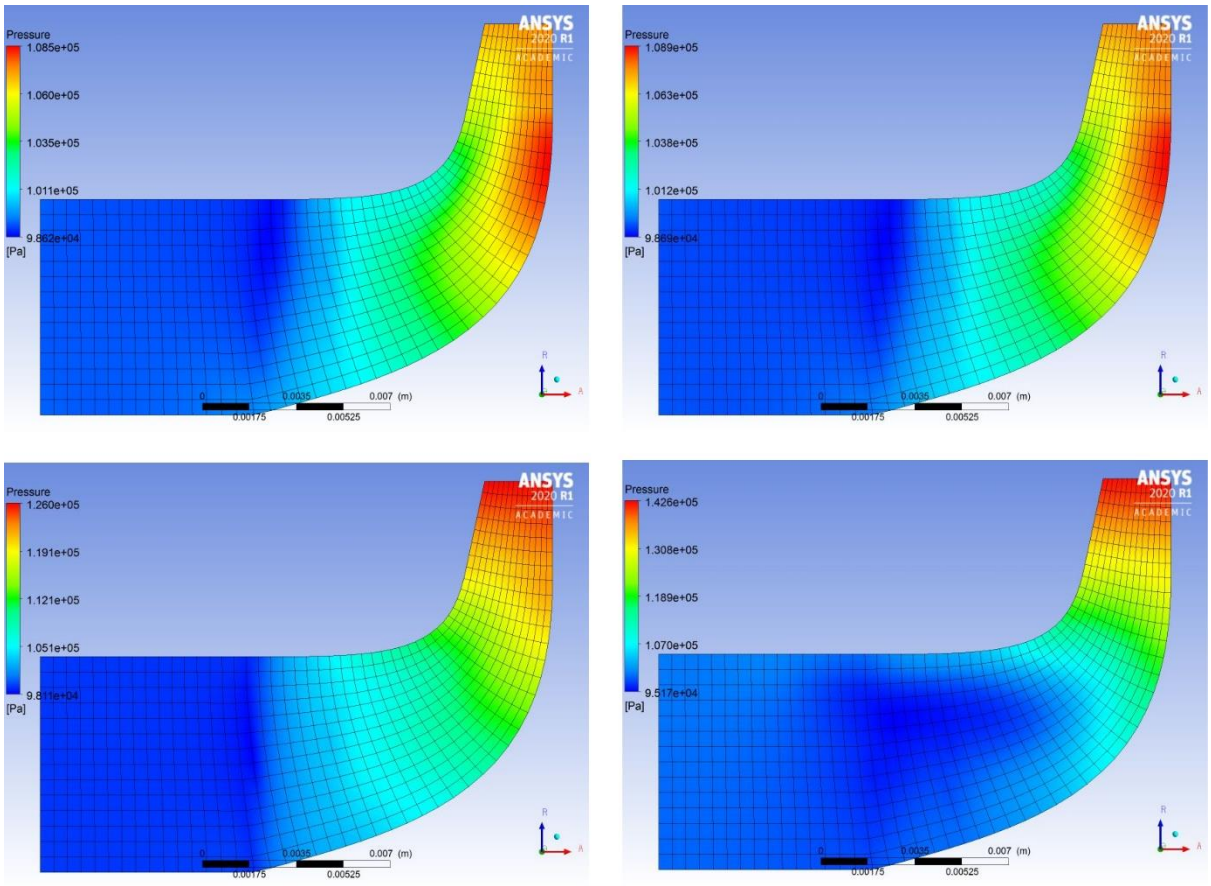

Fig. 8. Meridional view pressure distribution for T2 1.1 pressure ratio and T1 1.1, 1.3, 1.5 pressure ratio.

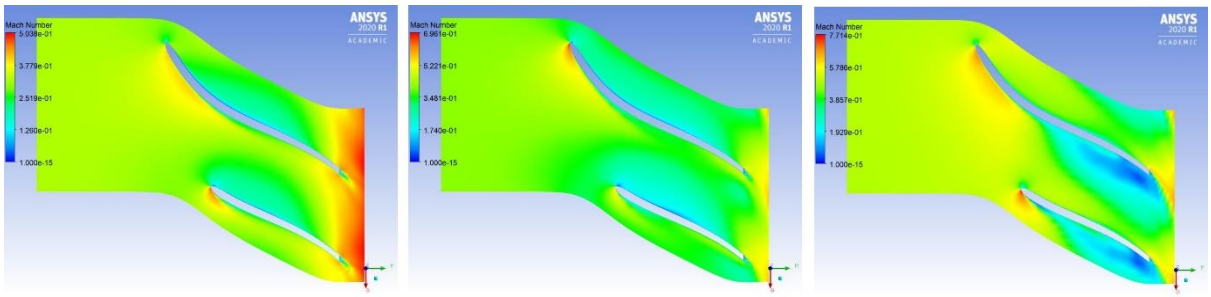

Fig. 9. Mach number distribution for T1 1.1, 1.3, 1.5 pressure ratio.

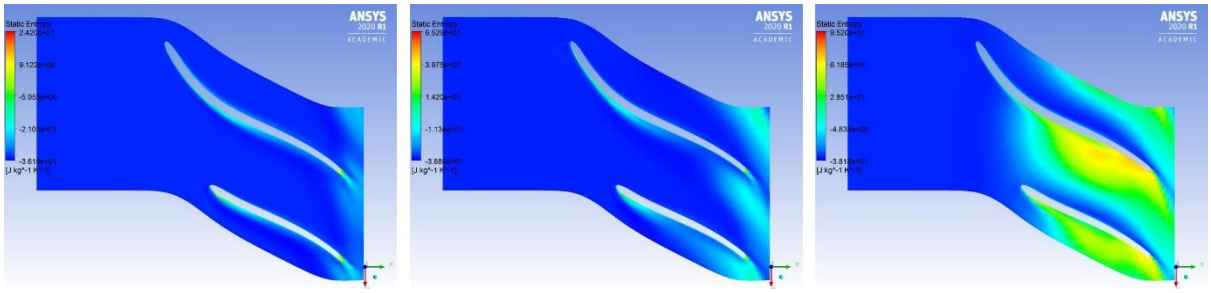

Fig. 10. Entropy distribution for T1 1.1, 1.3, 1.5 pressure ratio.

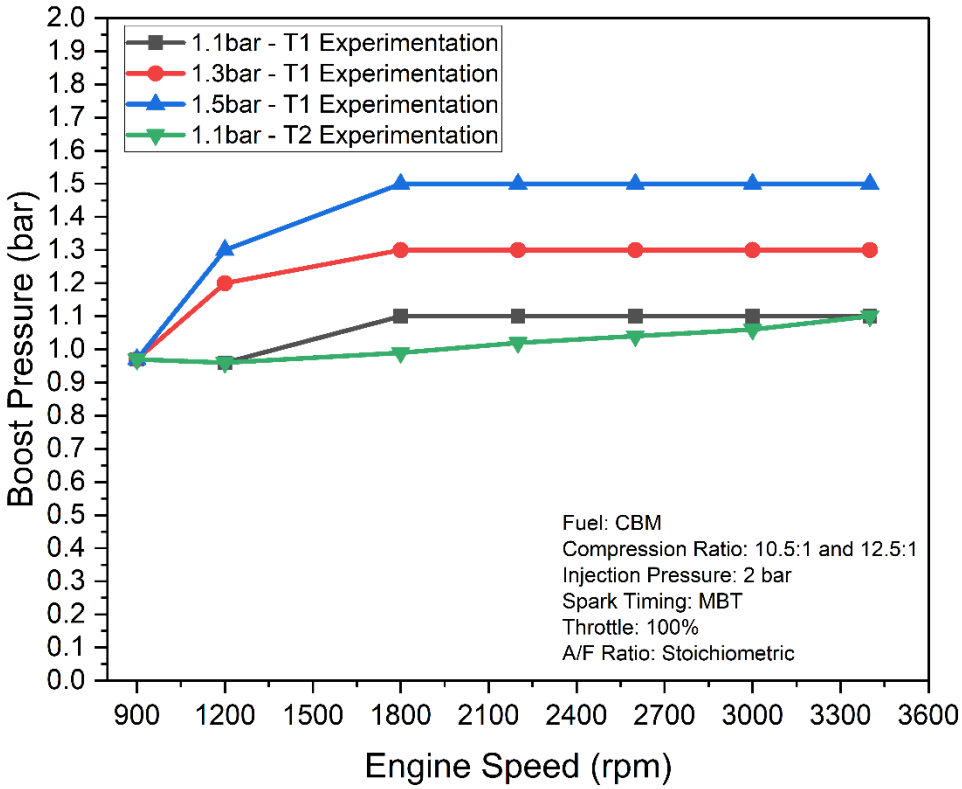

Fig. 11. Variation of boost pressure with engine speed.

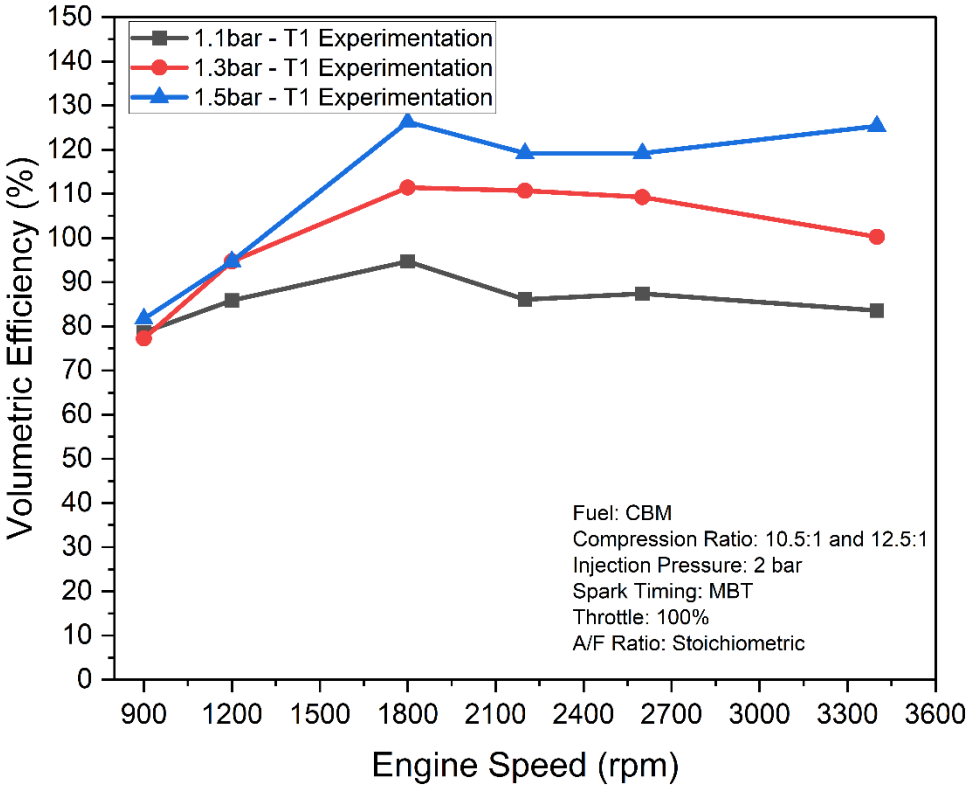

Fig. 12. Variation of volumetric efficiency with engine speed.

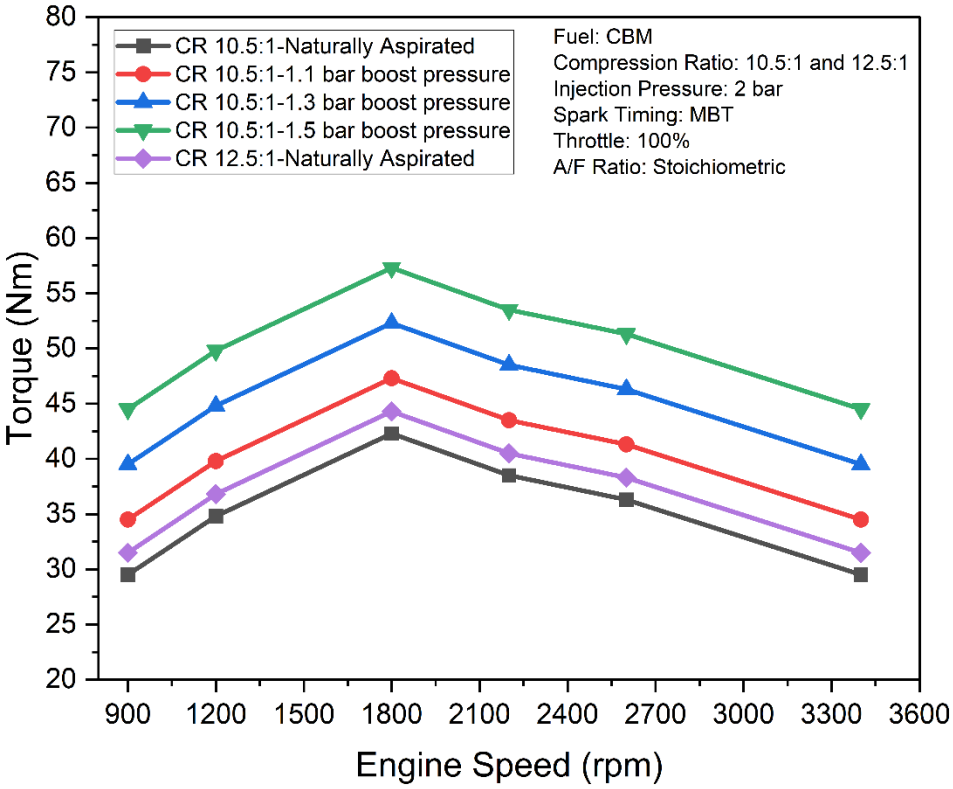

Fig. 13. Variation of torque with engine speed.

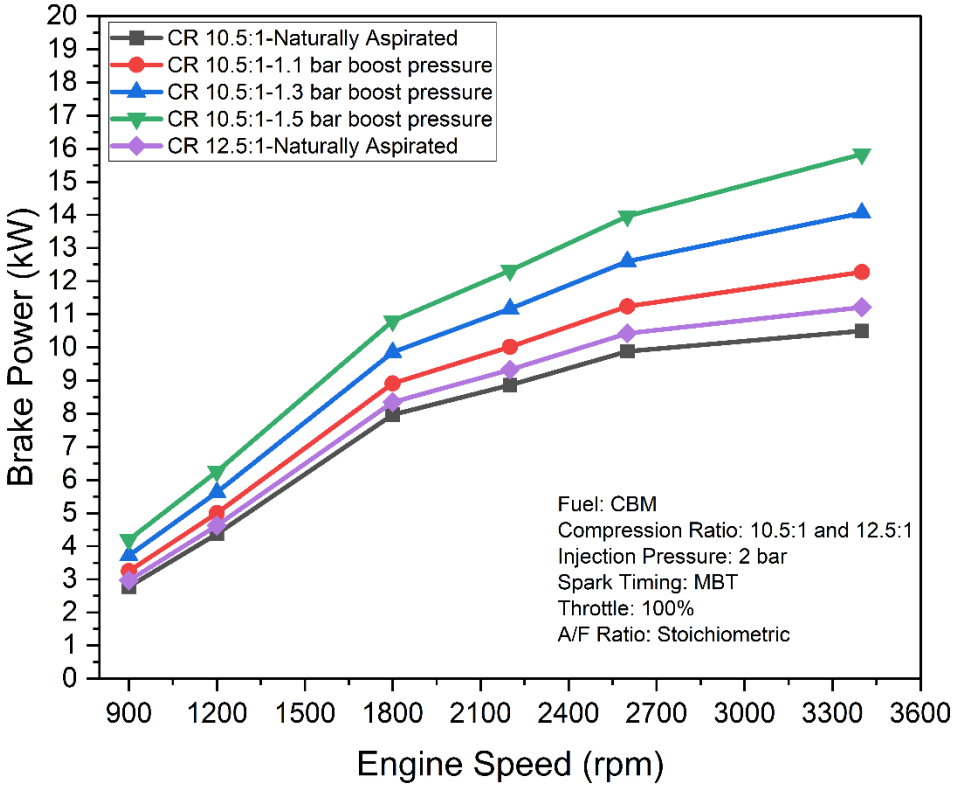

Fig. 14. Variation of brake power with engine speed.

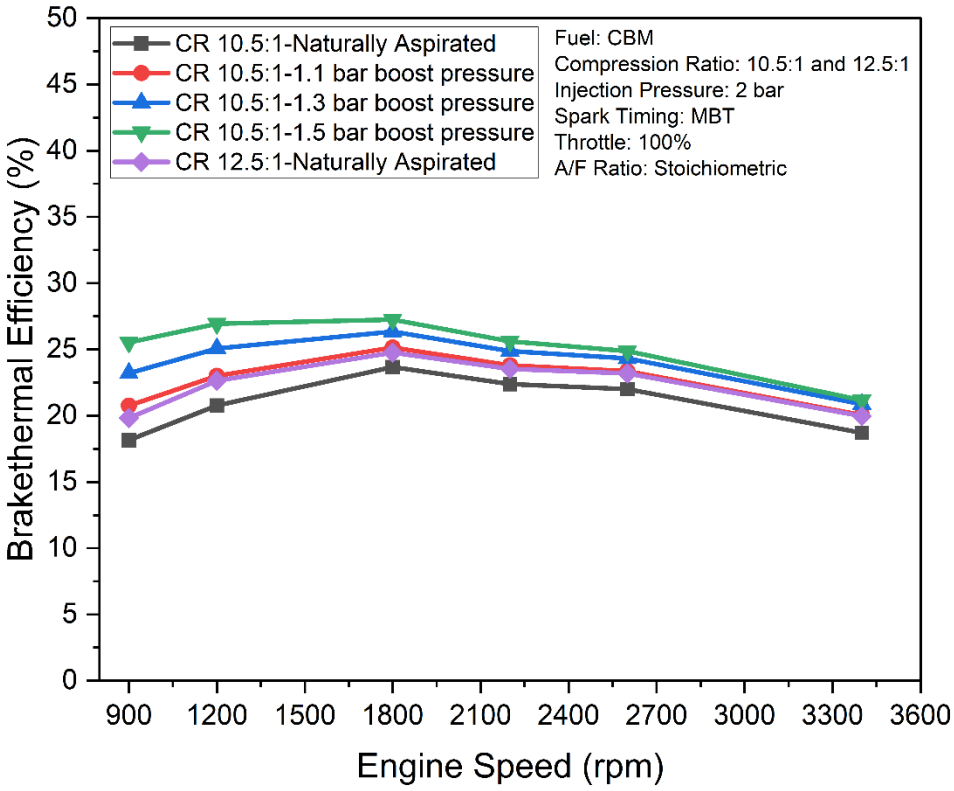

Fig. 15. Variation of brake thermal efficiency with engine speed.

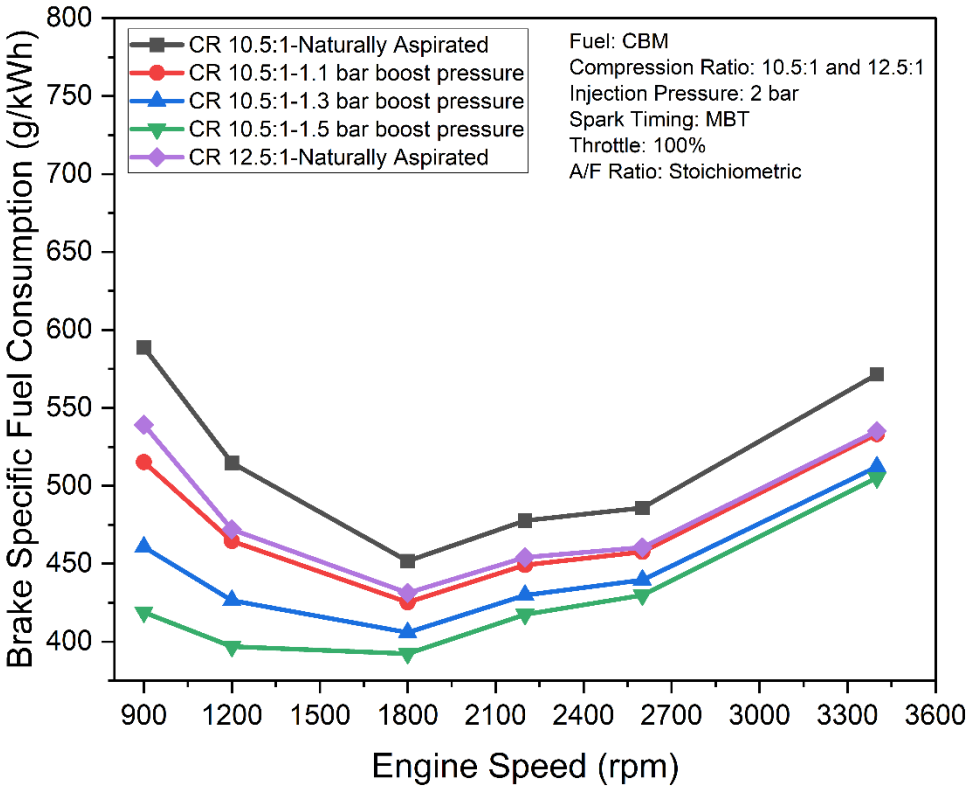

Fig. 16. Variation of brake specific fuel consumption with engine speed.

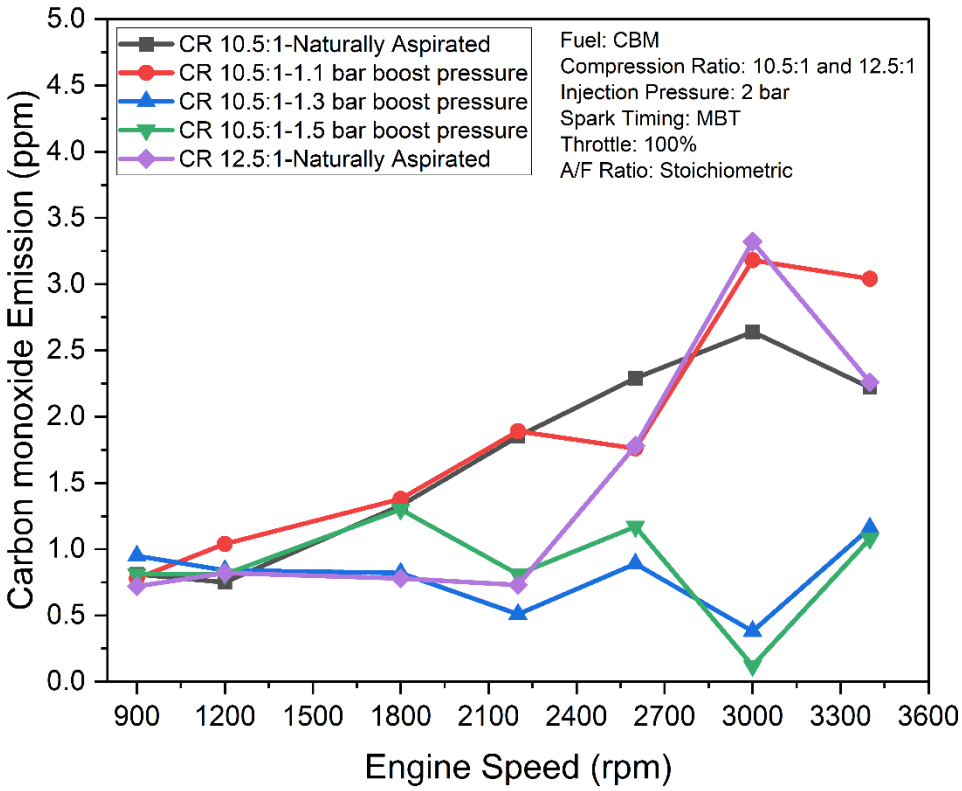

Fig. 17. Variation of CO emission with engine speed.

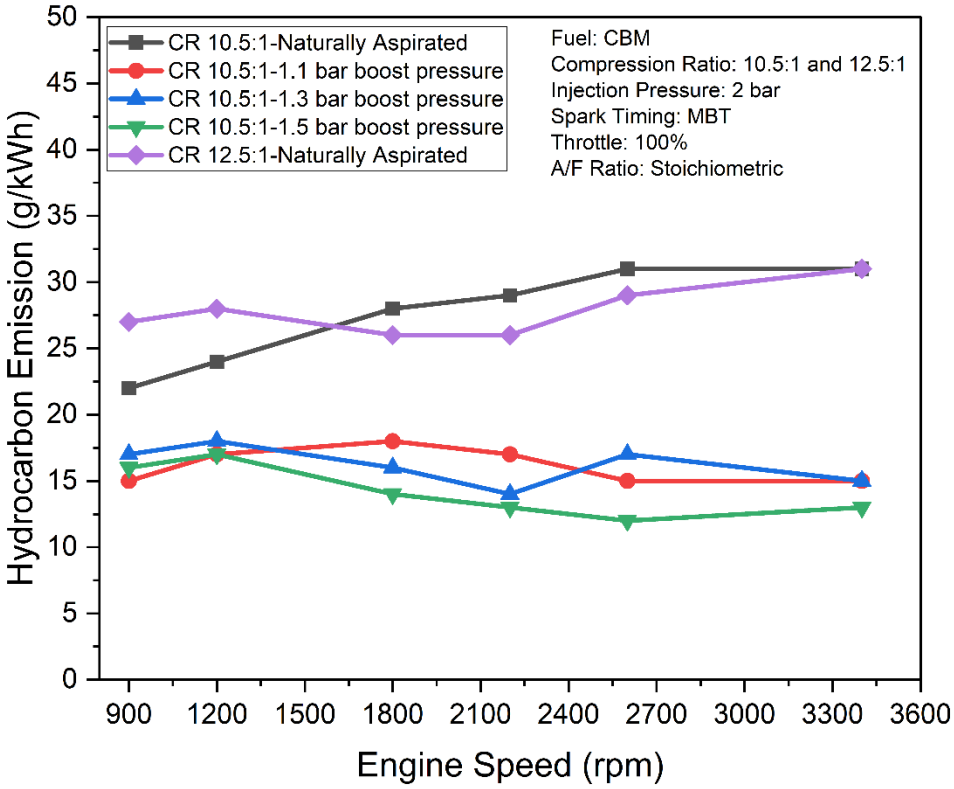

Fig. 18. Variation of HC emission with engine speed.

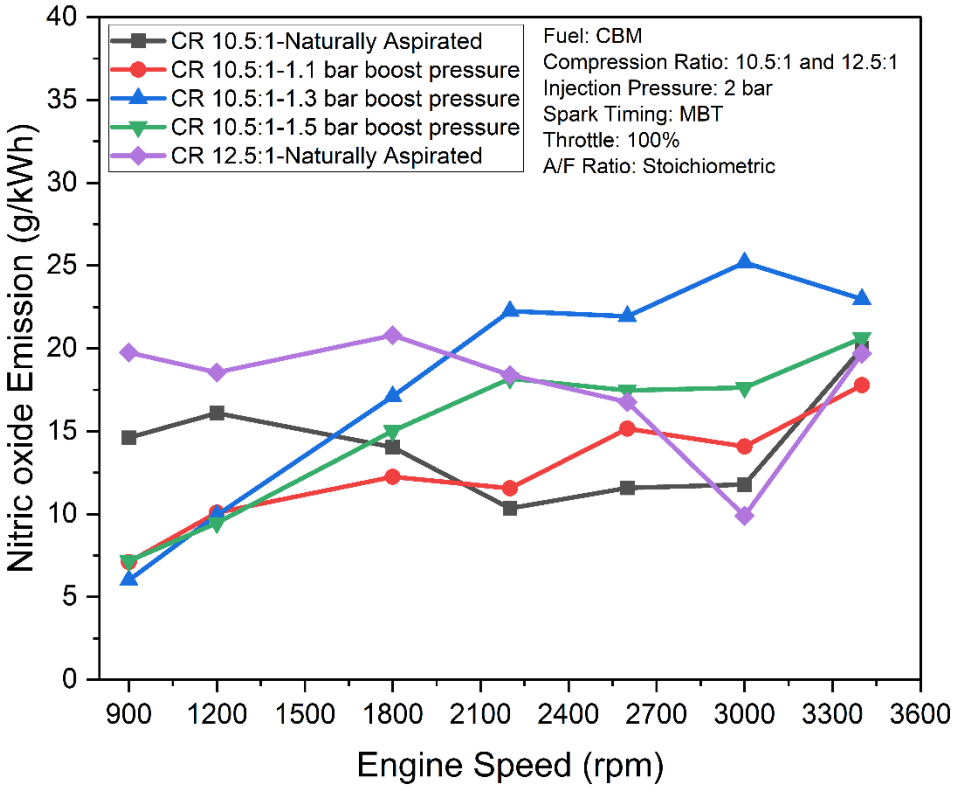

Fig. 19. Variation of NO emission with engine speed.

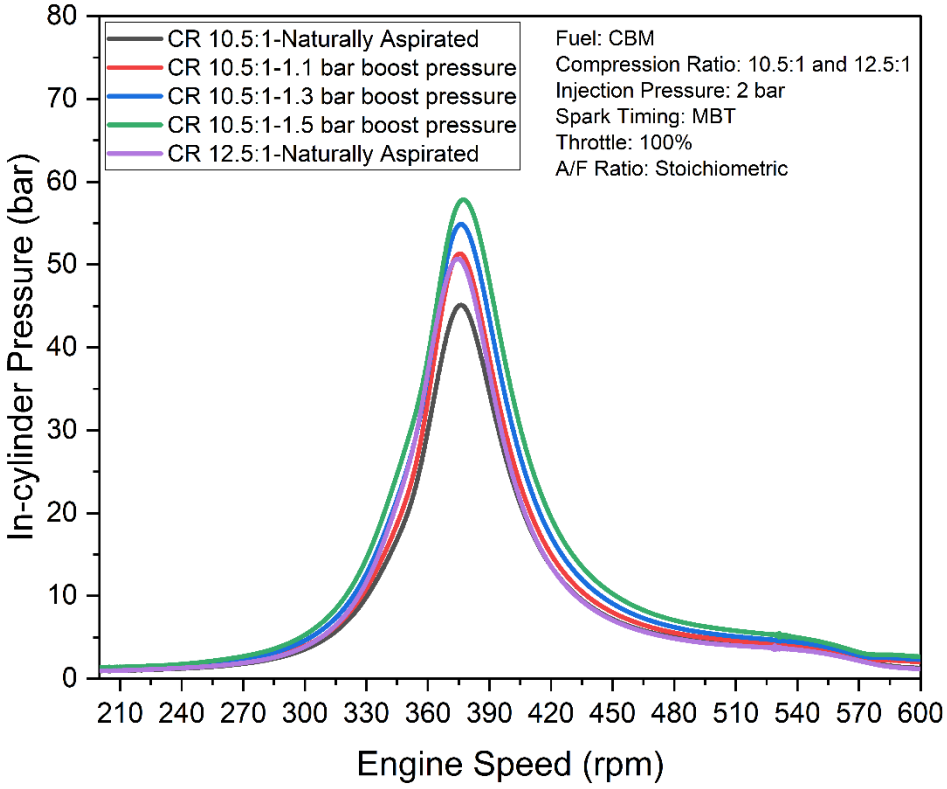

Fig. 20. Variation of in-cylinder pressure with engine speed.

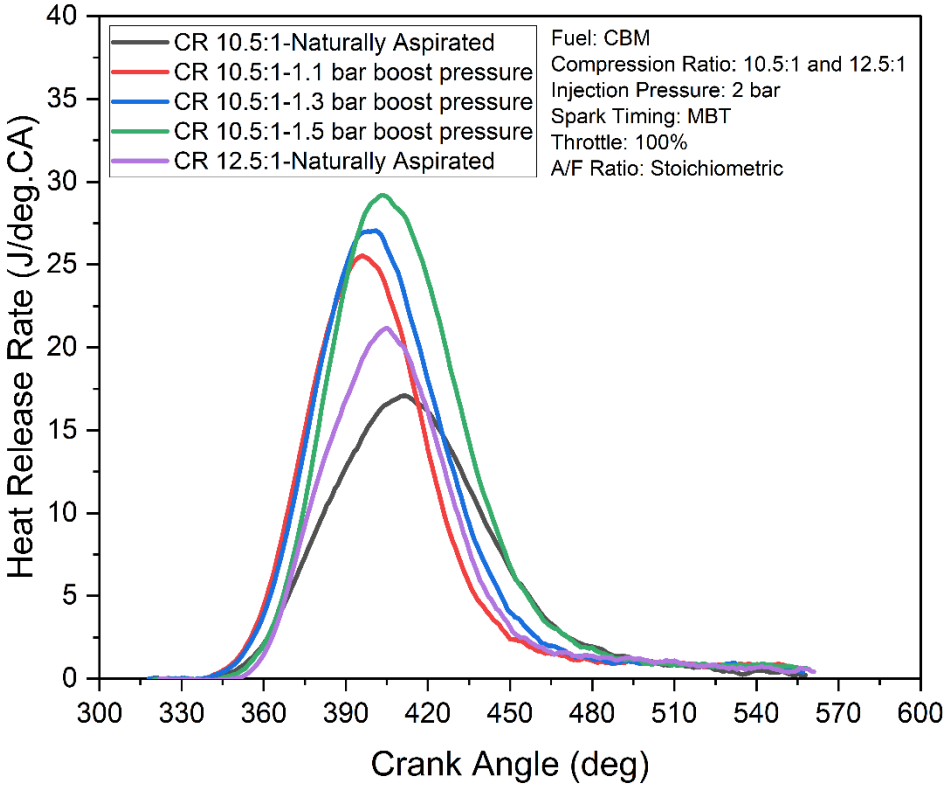

Fig. 21. Variation of heat release rate with crank angle.

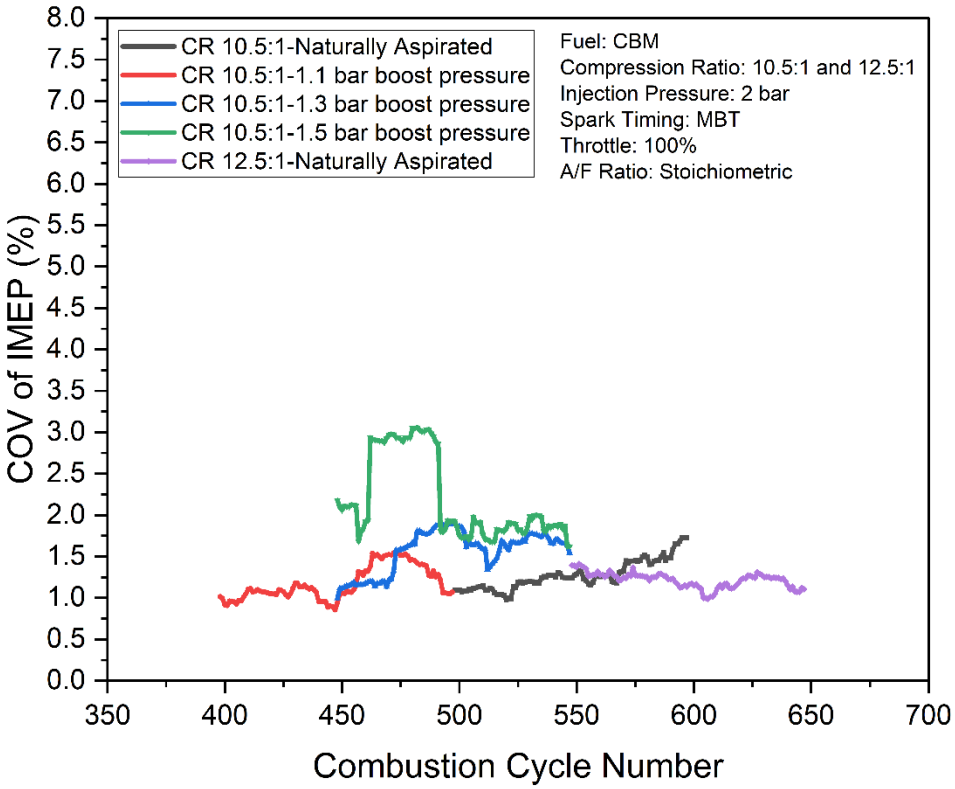

Fig. 22. Variation of COV of IMEP with combustion cycle number.

Figures

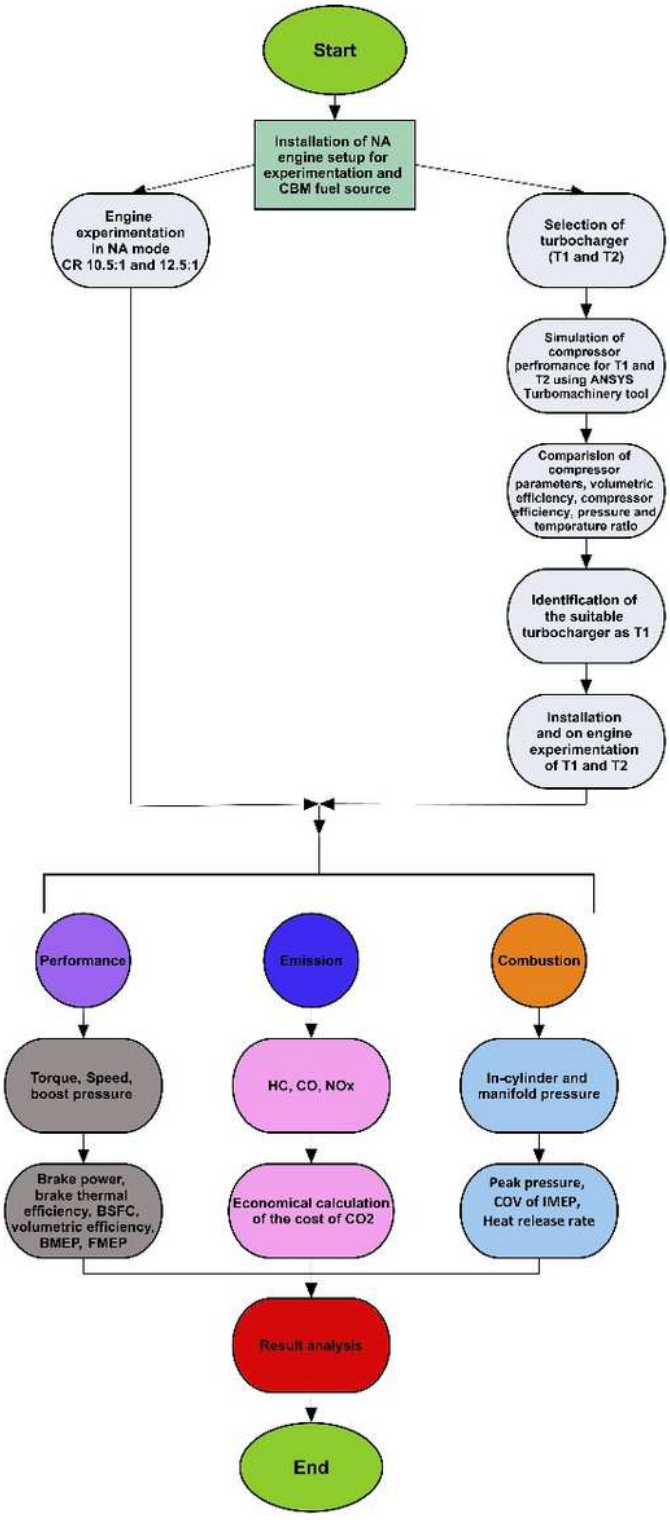

Figure 1

Test plan for simulation and experimental procedures.

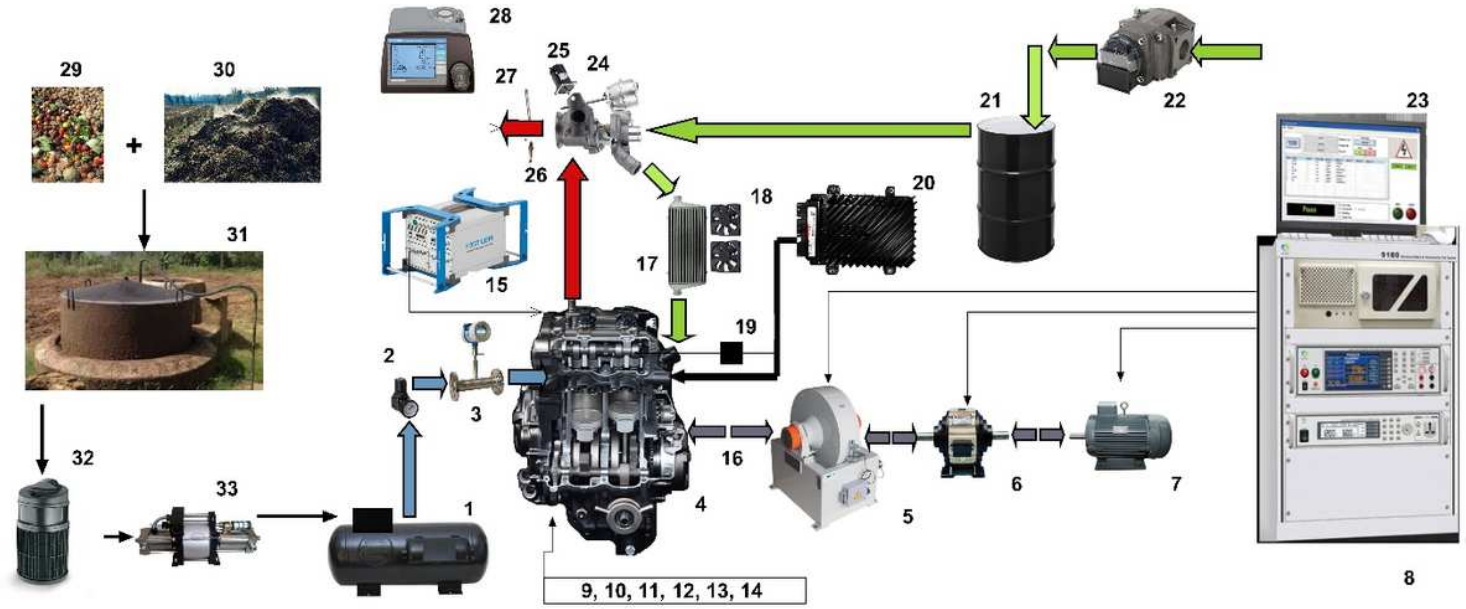

Figure 2

Schematic layout of the experimental setup.

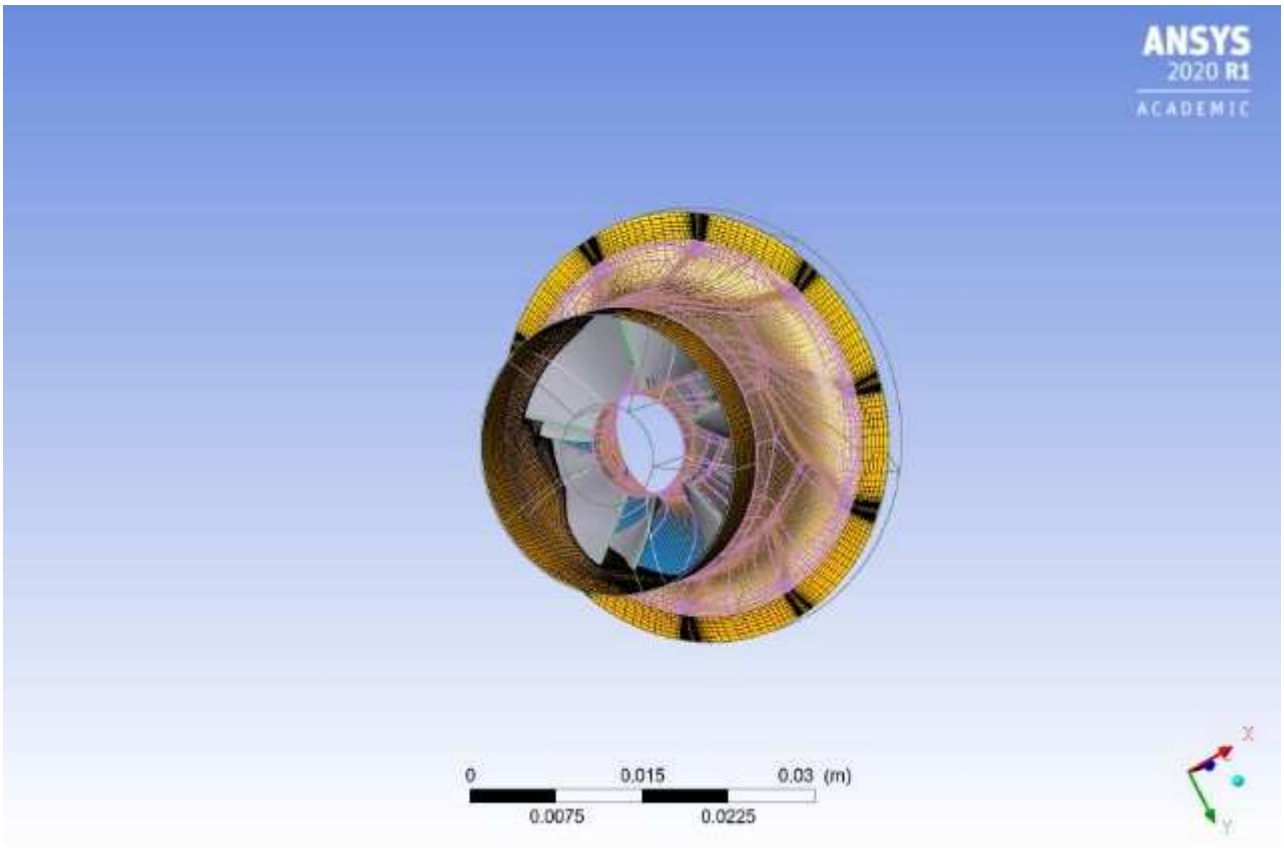

Figure 3

Meshed view of the compressor impeller.

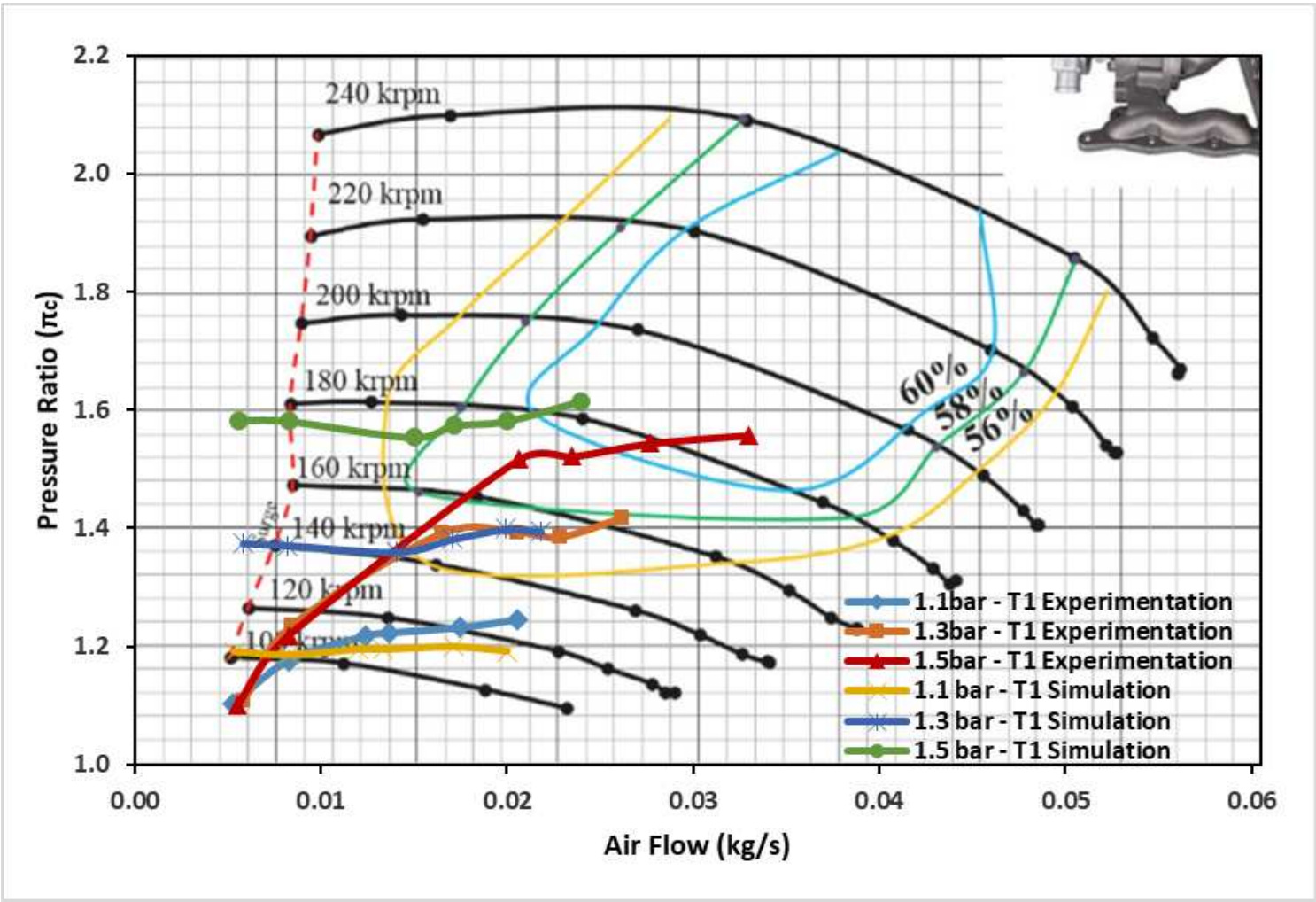

Figure 4

Variation of pressure ratio with airflow for T1.

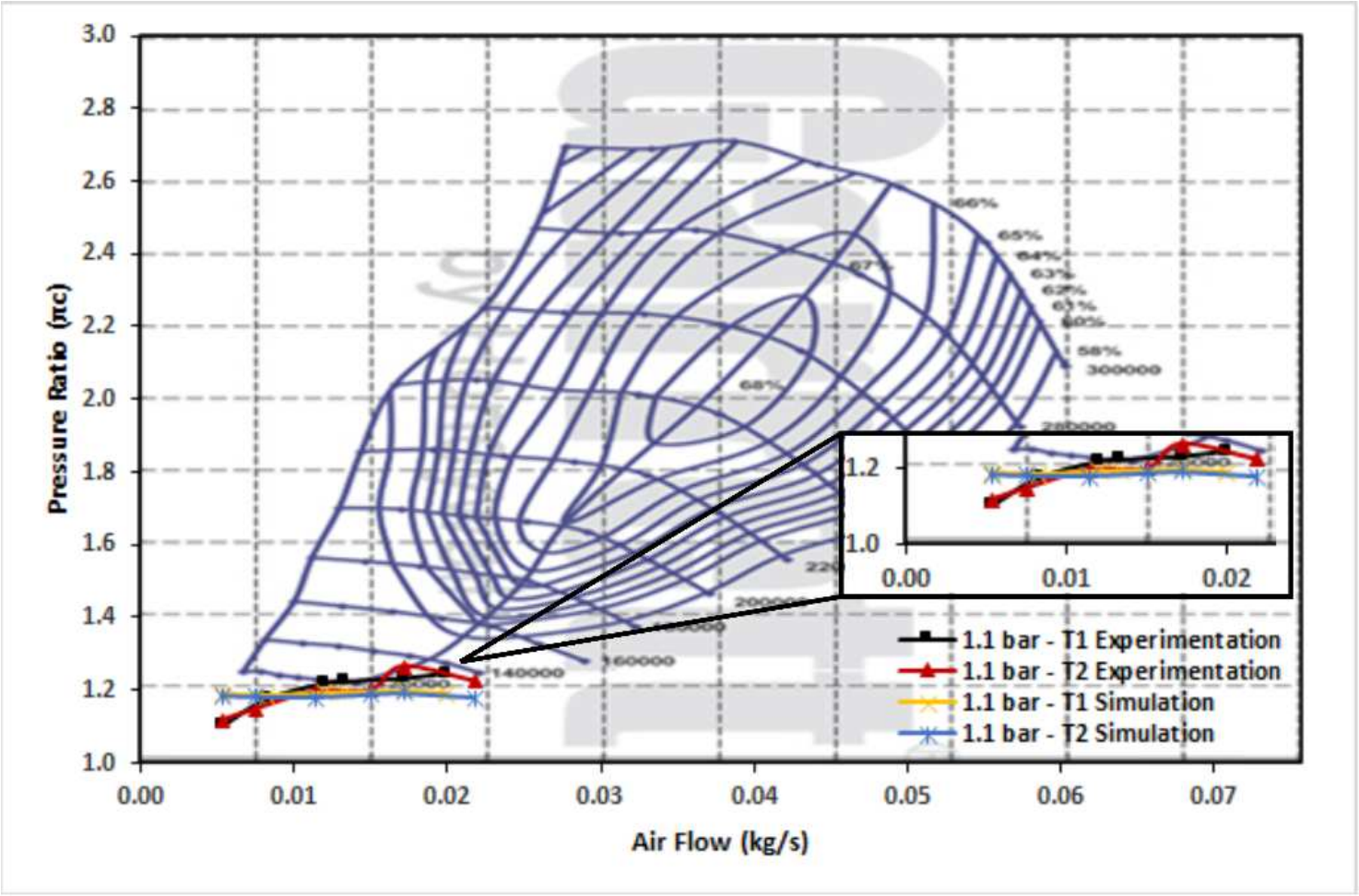

Figure 5

Variation of pressure ratio with airflow for T2.

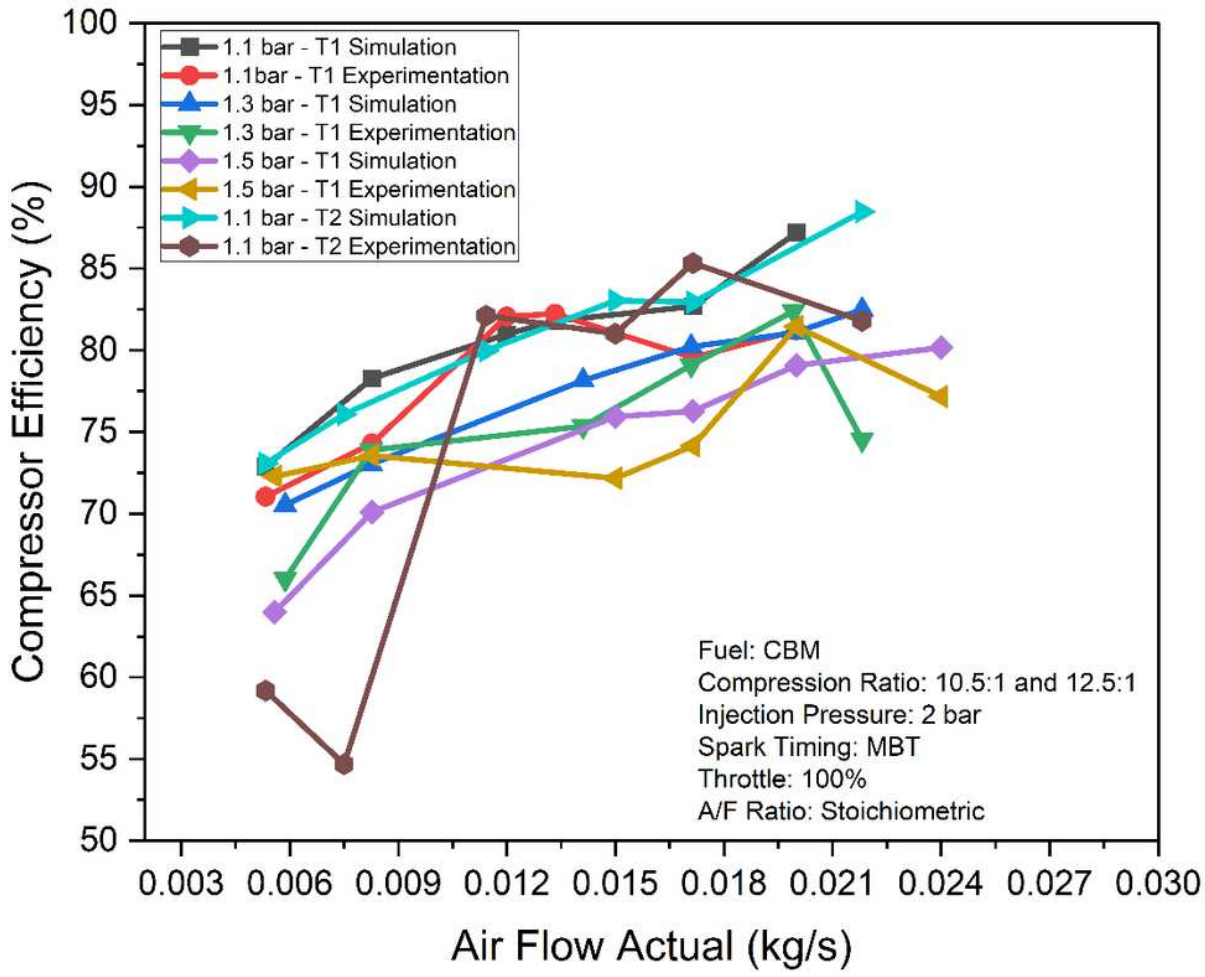

Figure 6

Variation of compressor efficiency with airflow for T1.

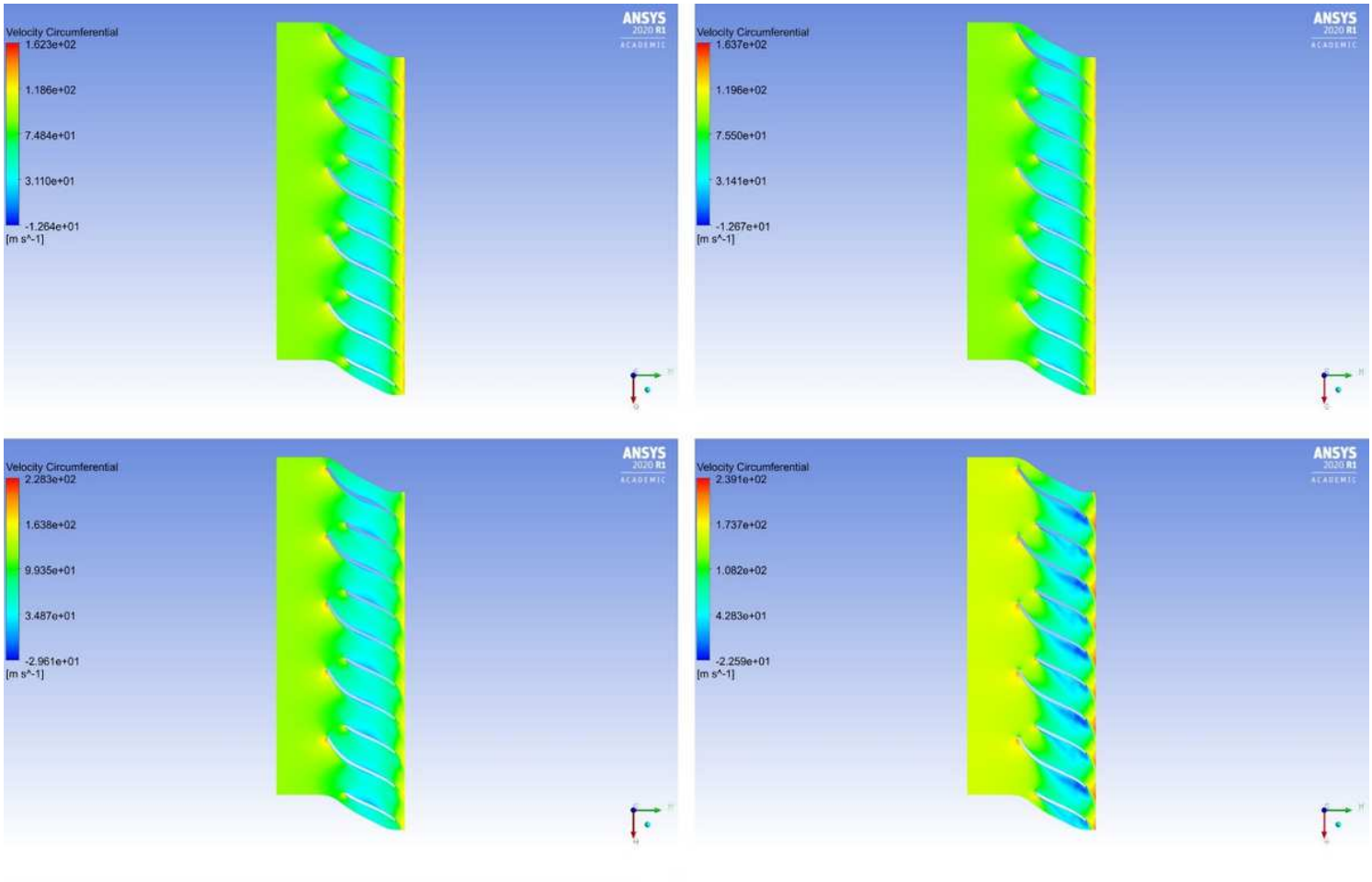

Figure 7

Blade to blade view ccircumferential velocity distribution for T2 1.1 pressure ratio and T1 1.1, 1.3, 1.5 pressure ratio.

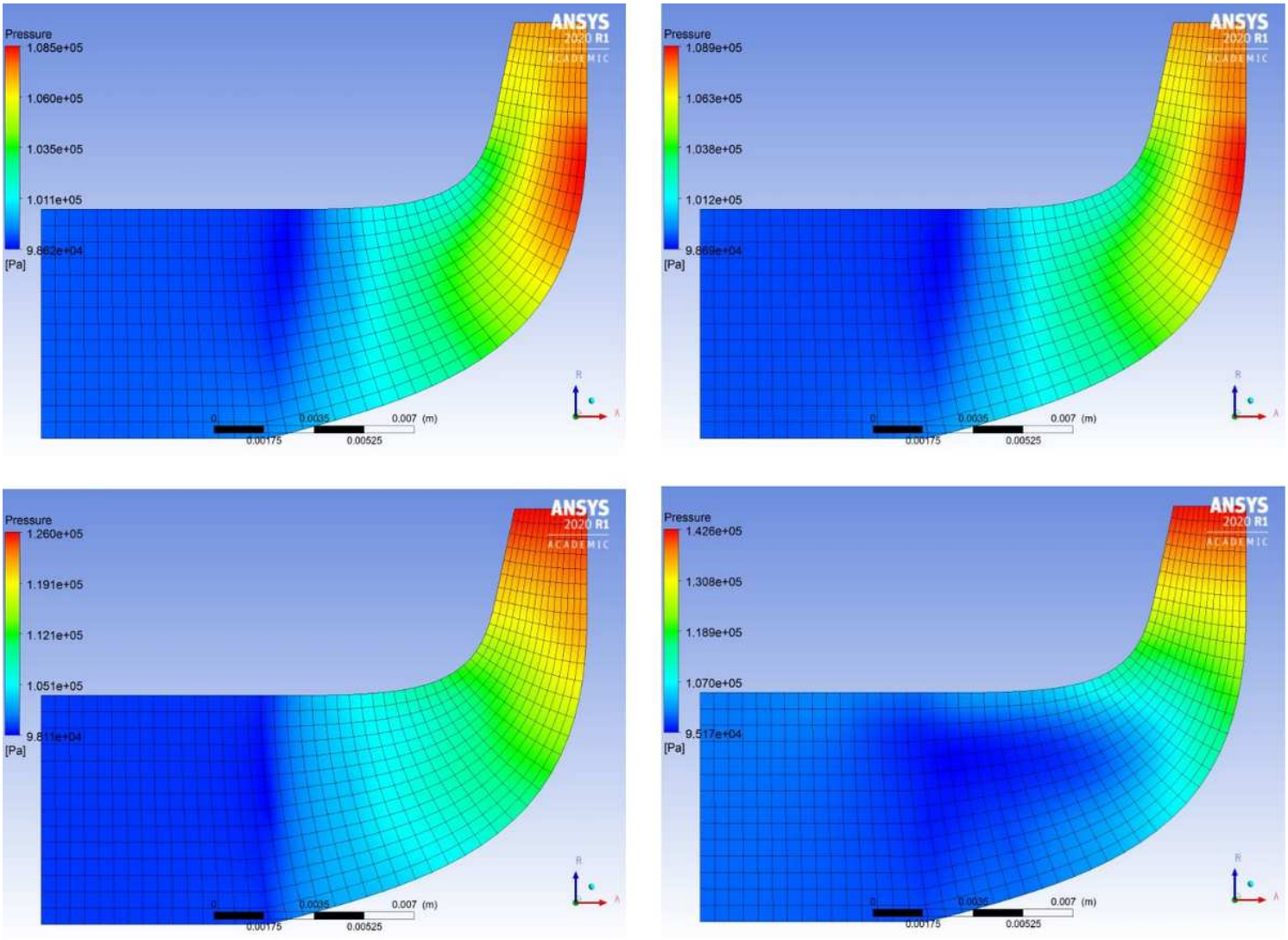

Figure 8

Meridional view pressure distribution for T2 1.1 pressure ratio and T1 1.1, 1.3, 1.5 pressure ratio.

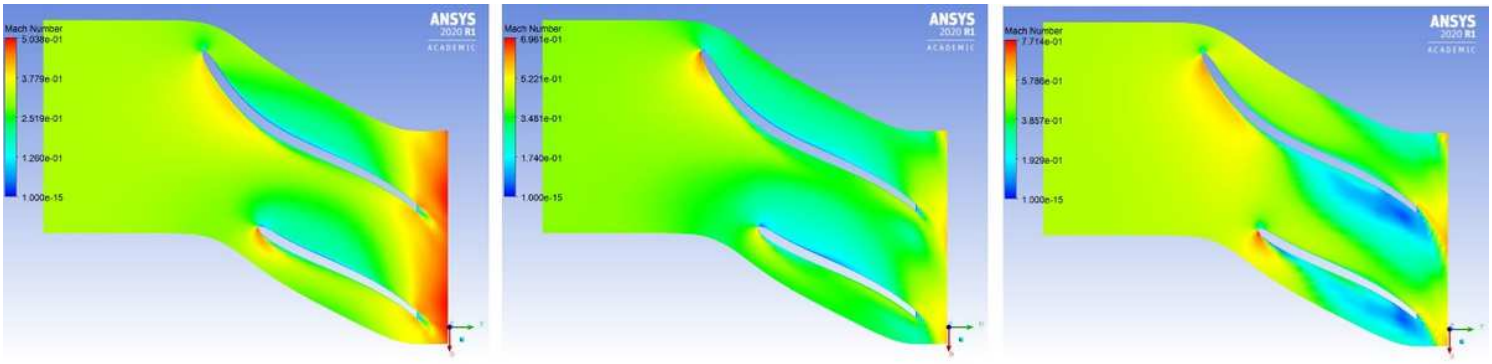

Figure 9

Mach number distribution for T1 1.1, 1.3, 1.5 pressure ratio.

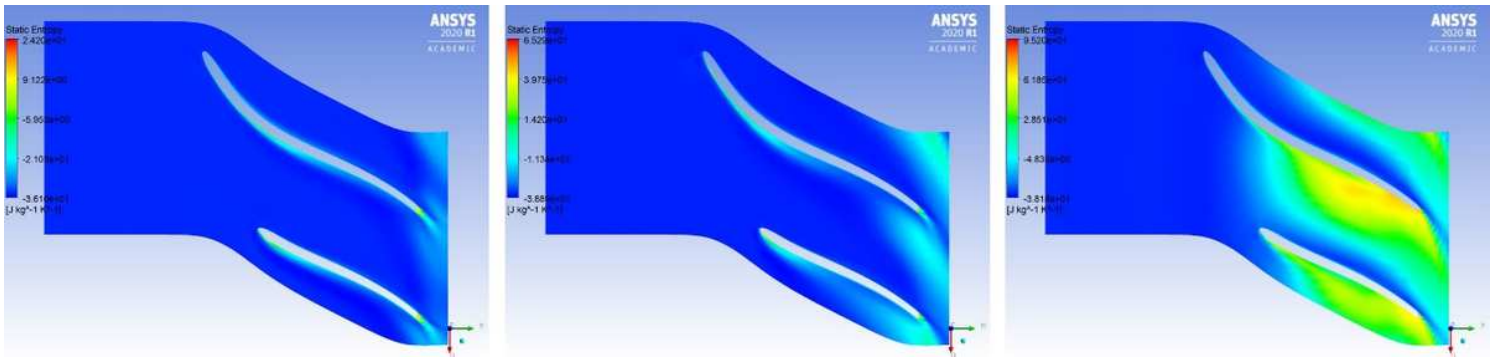

Figure 10

Entropy distribution for T1 1.1, 1.3, 1.5 pressure ratio.

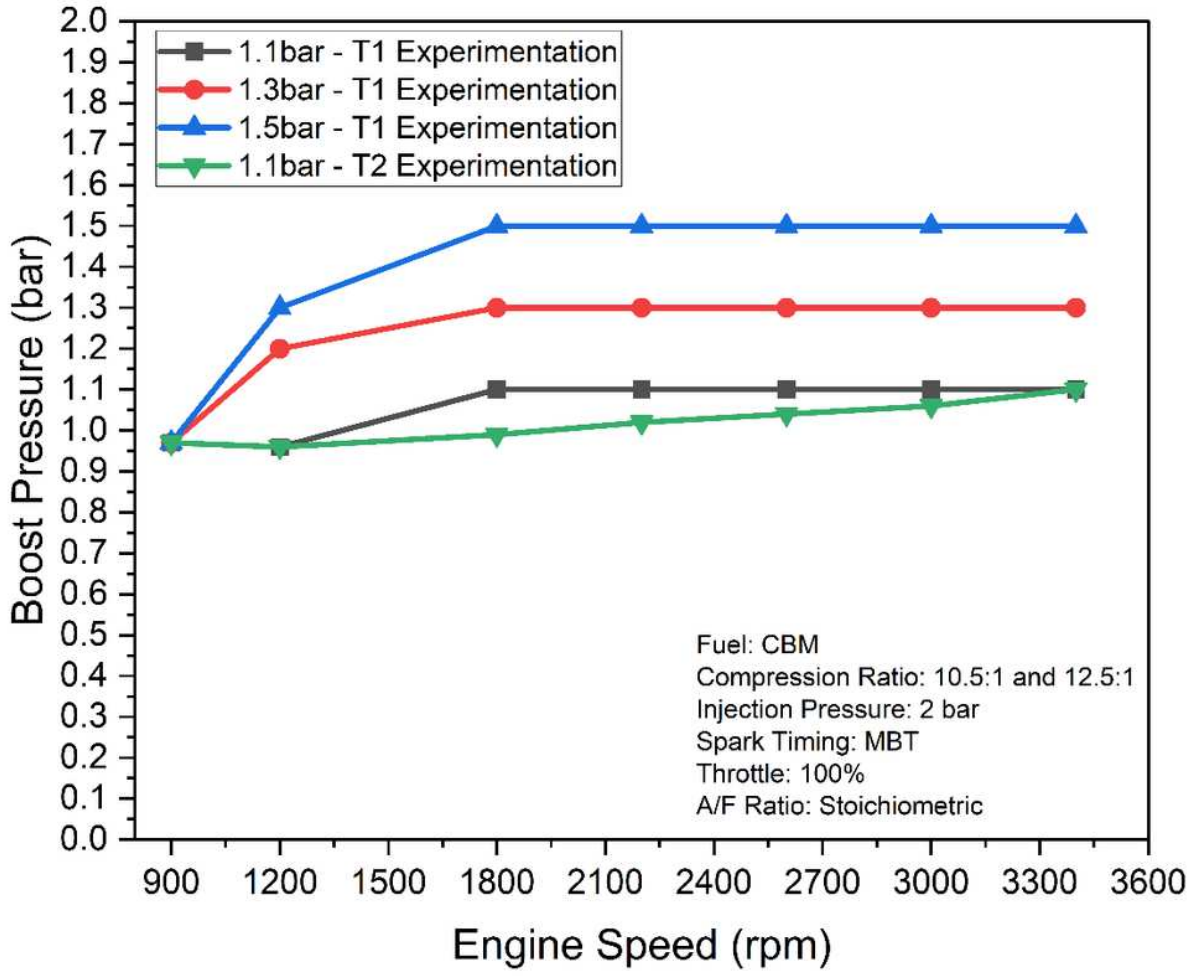

Figure 11

Variation of boost pressure with engine speed.

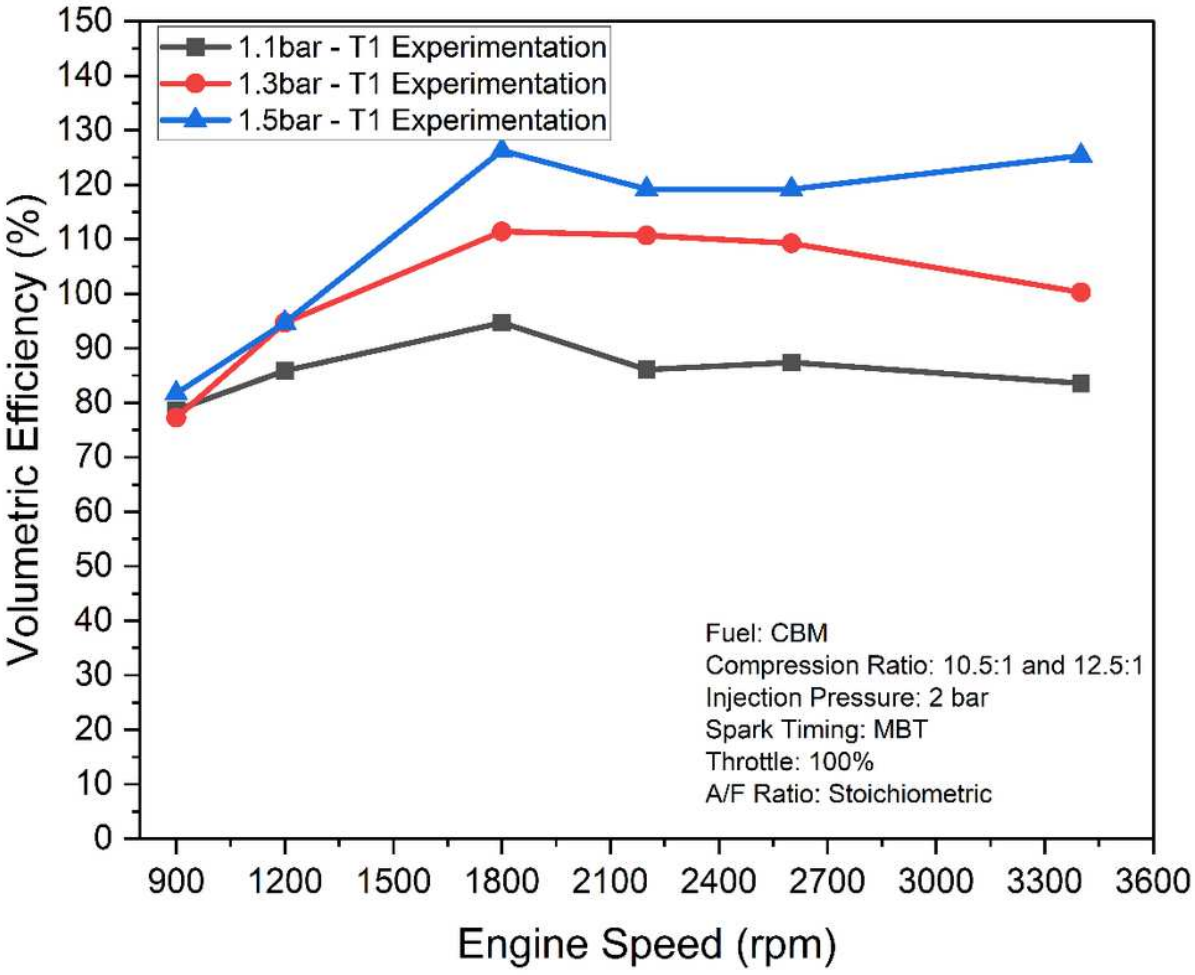

Figure 12

Variation of volumetric efficiency with engine speed.

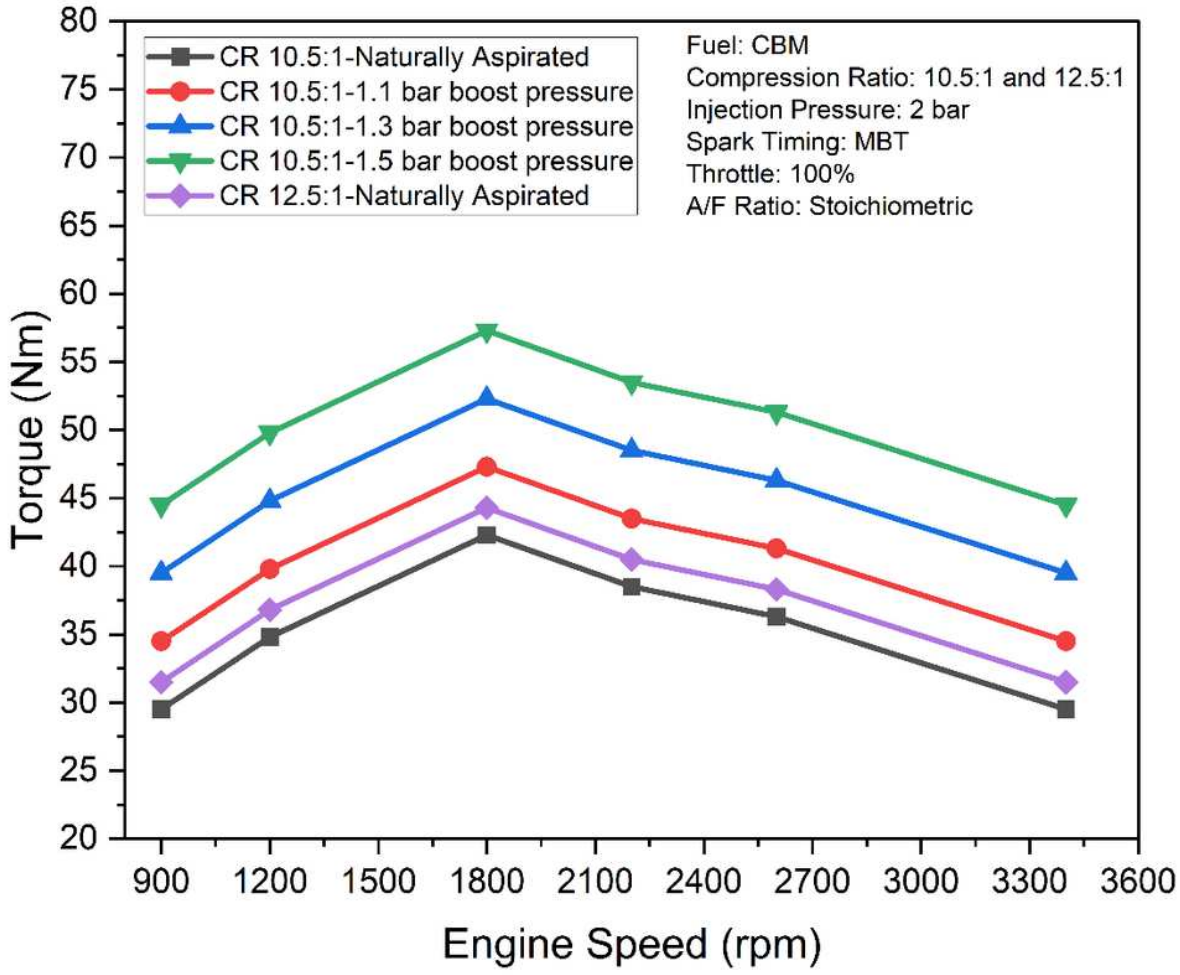

Figure 13

Variation of torque with engine speed.

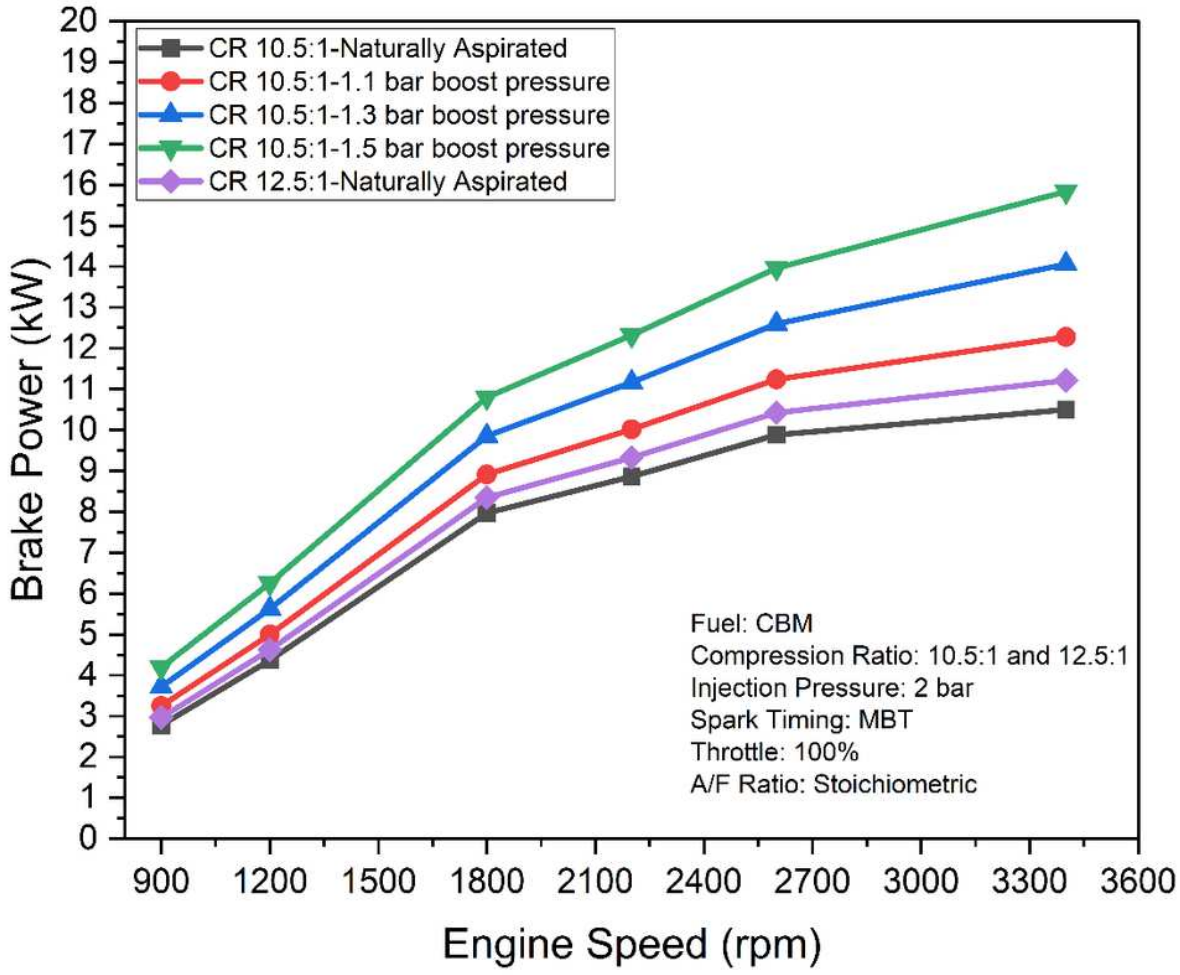

Figure 14

Variation of brake power with engine speed.

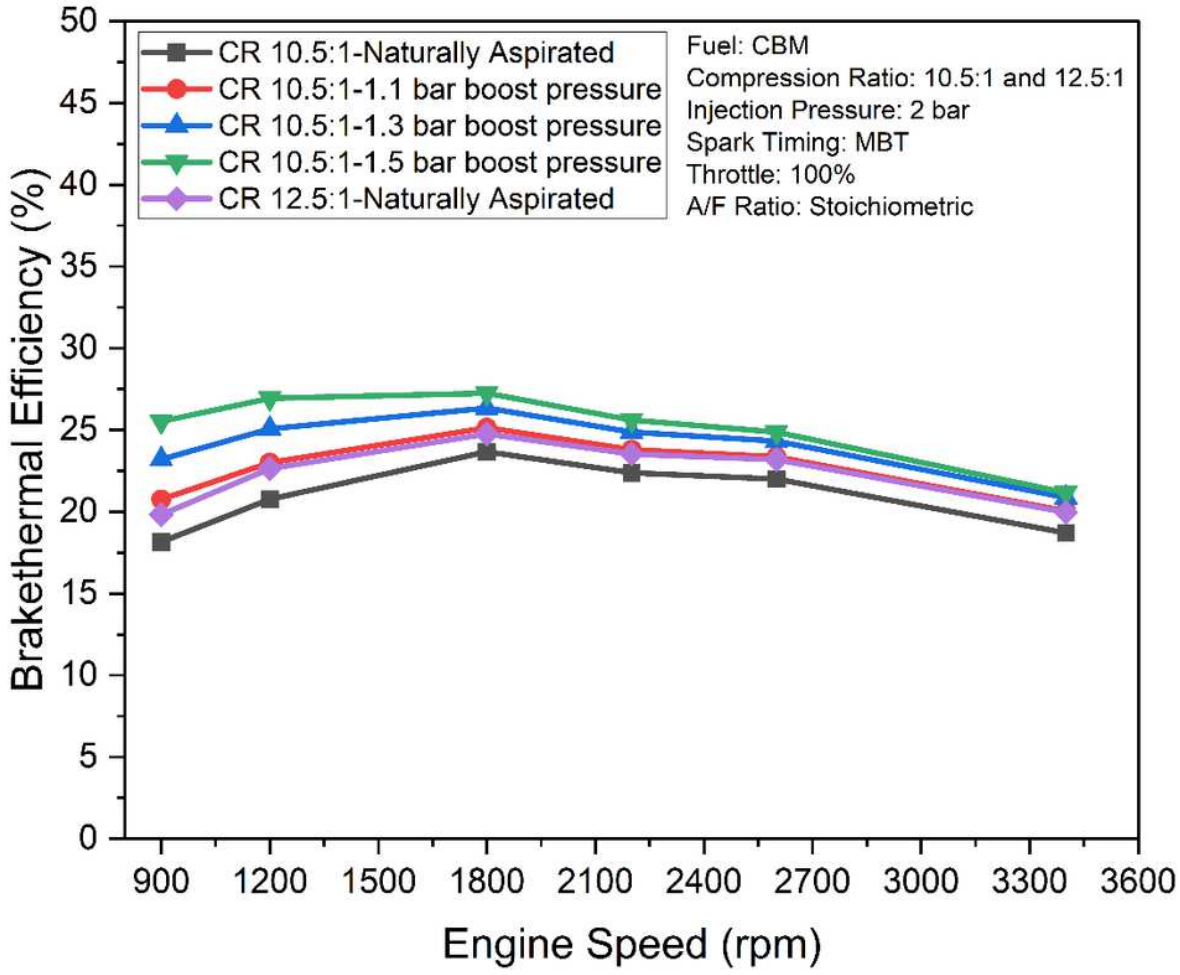

Figure 15

Variation of brake thermal efficiency with engine speed.

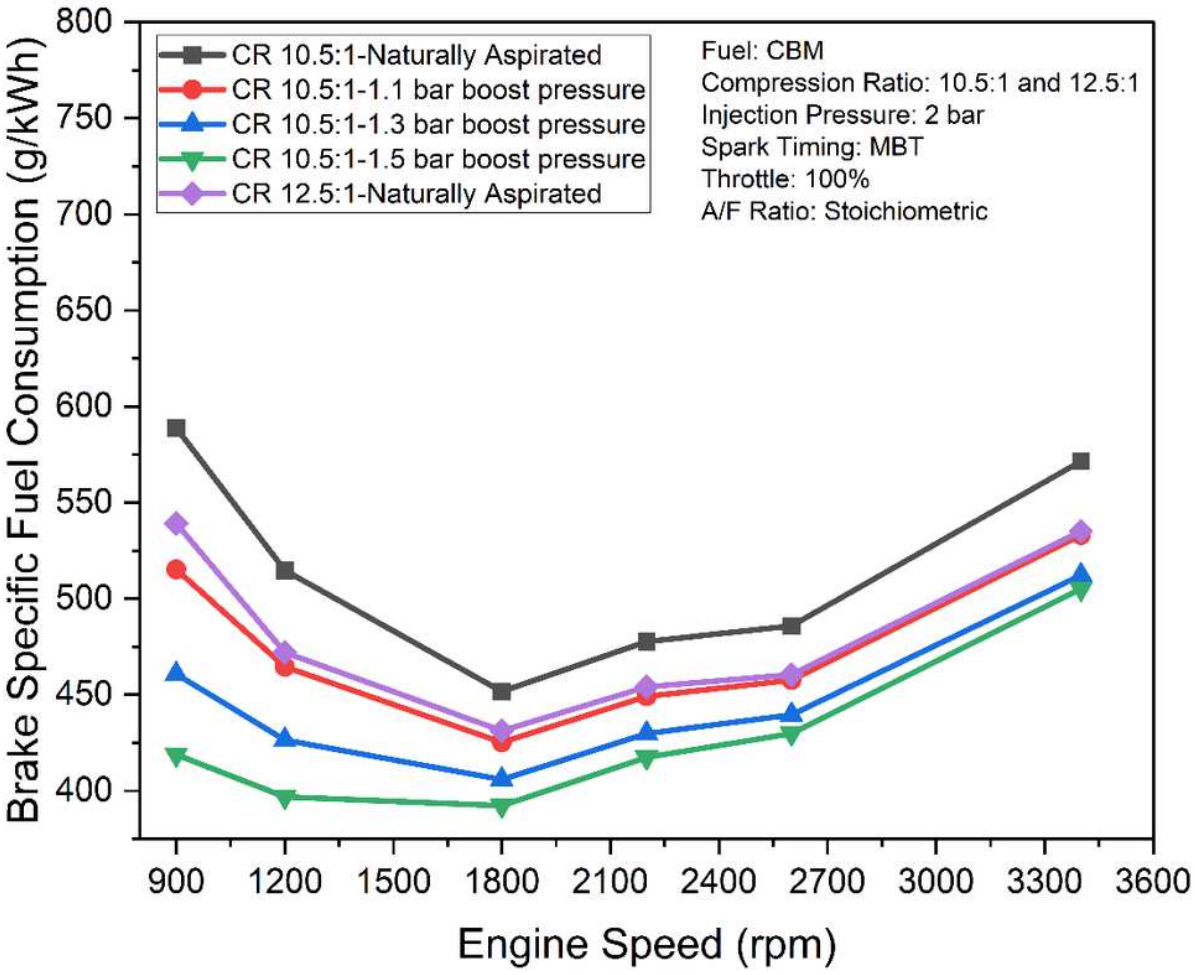

Figure 16

Variation of brake specific fuel consumption with engine speed.

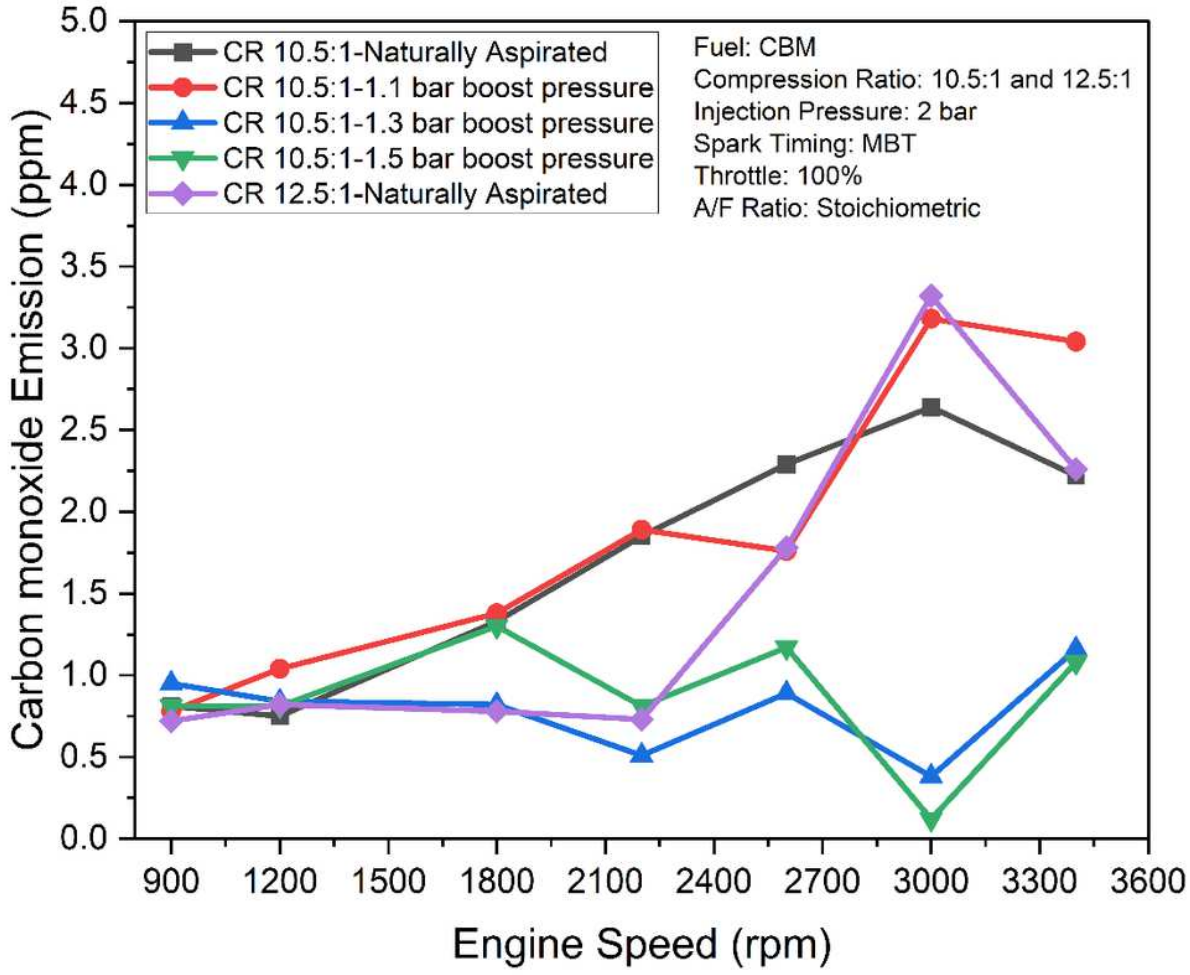

Figure 17

Variation of CO emission with engine speed.

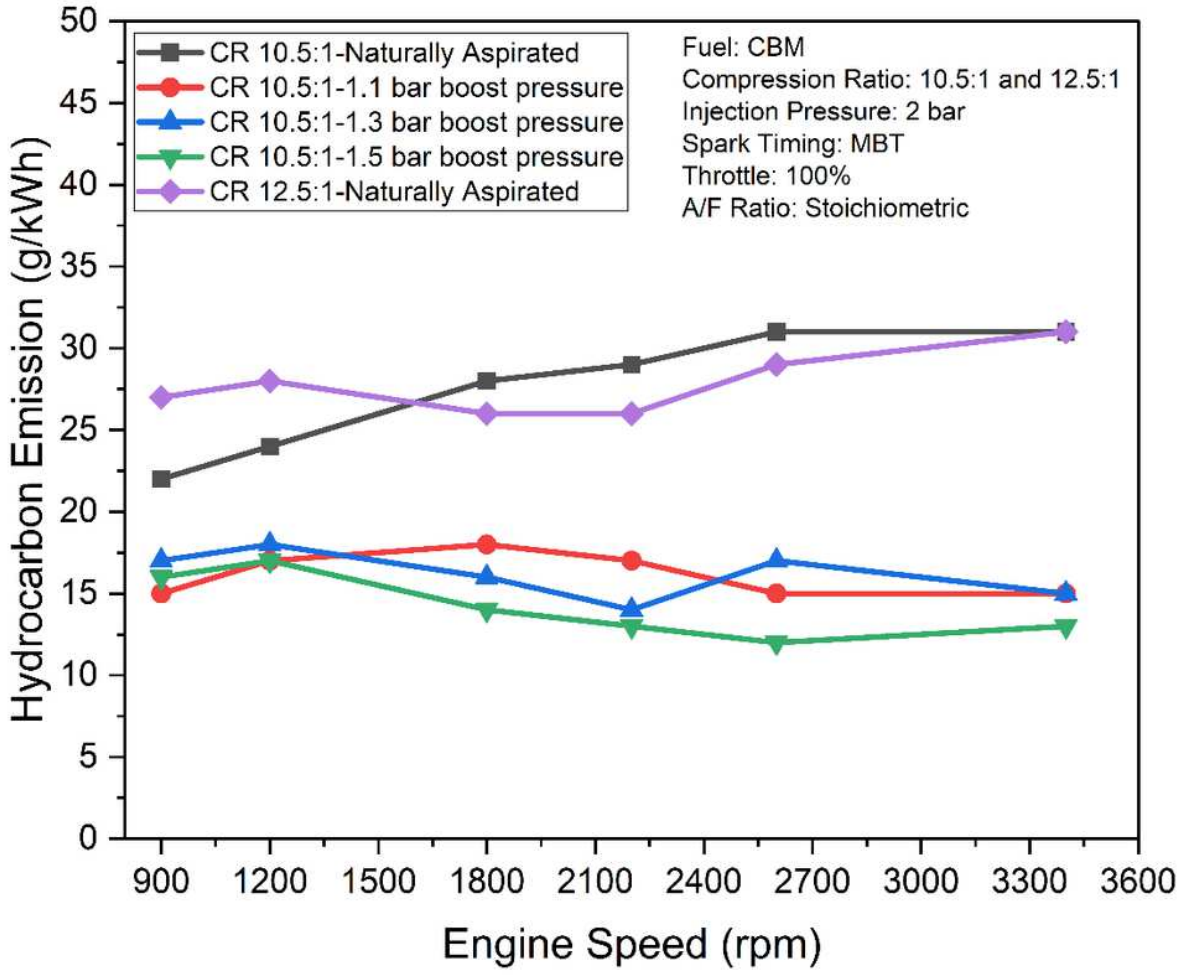

Figure 18

Variation of HC emission with engine speed.

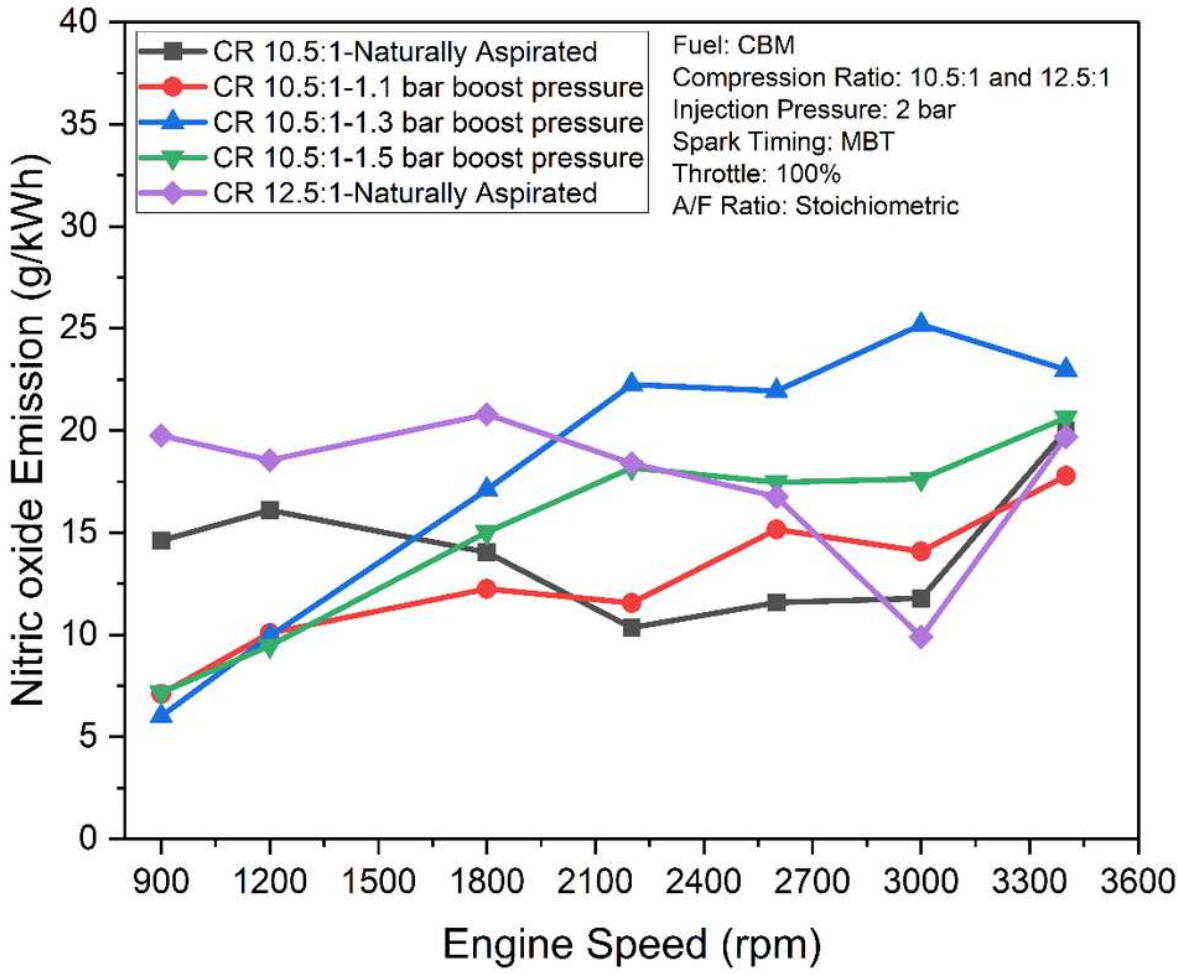

Figure 19

Variation of NO emission with engine speed.

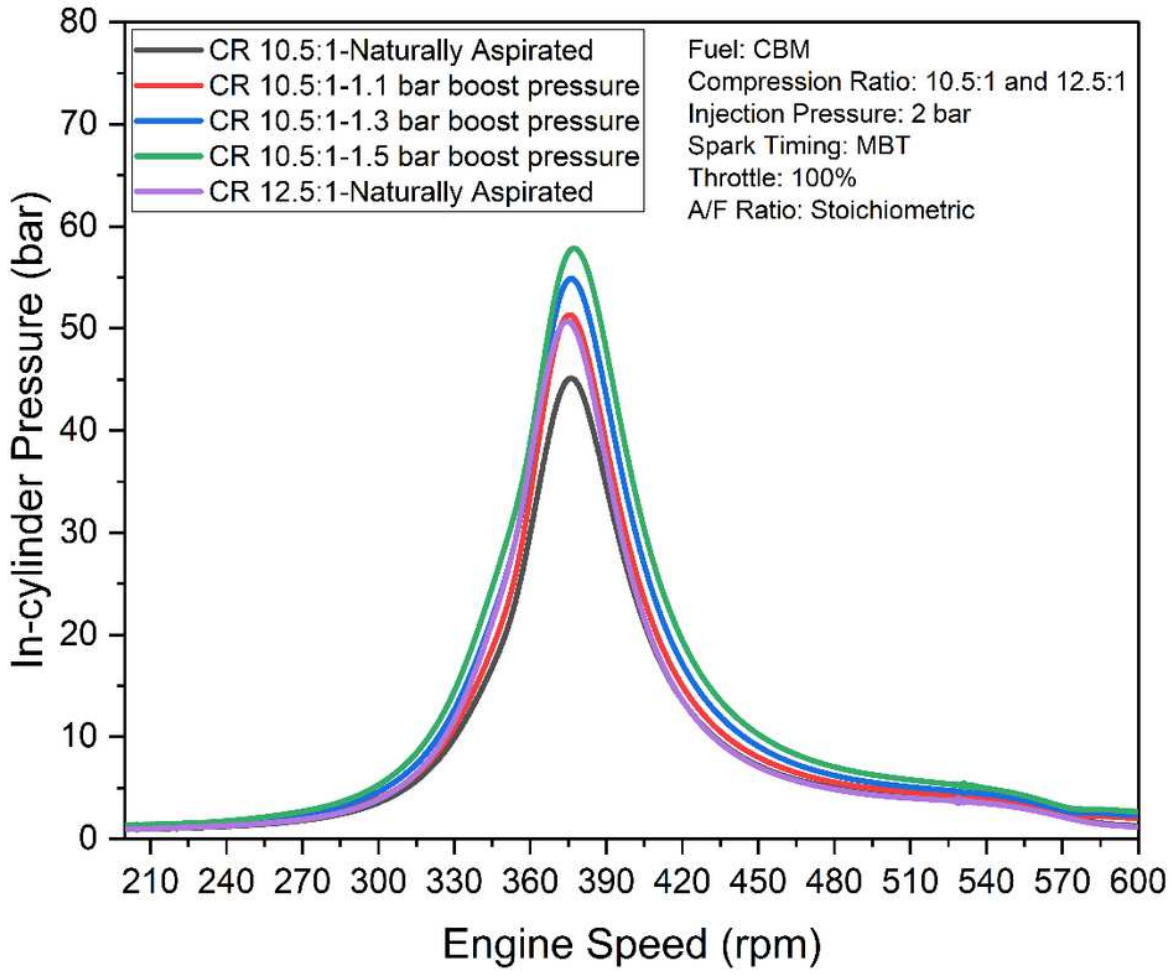

Figure 20

Variation of in-cylinder pressure with crank angle.

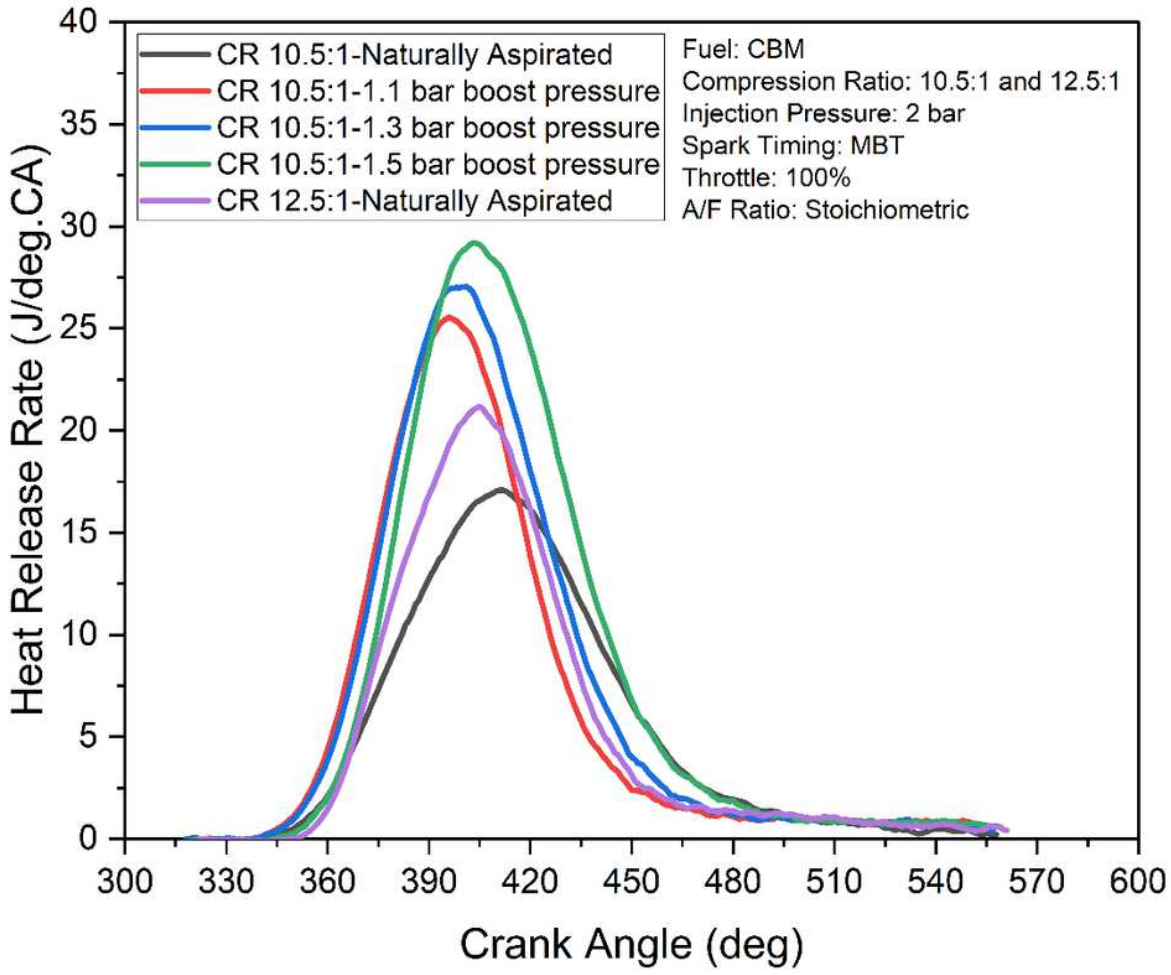

Figure 21

Variation of heat release rate with crank angle.

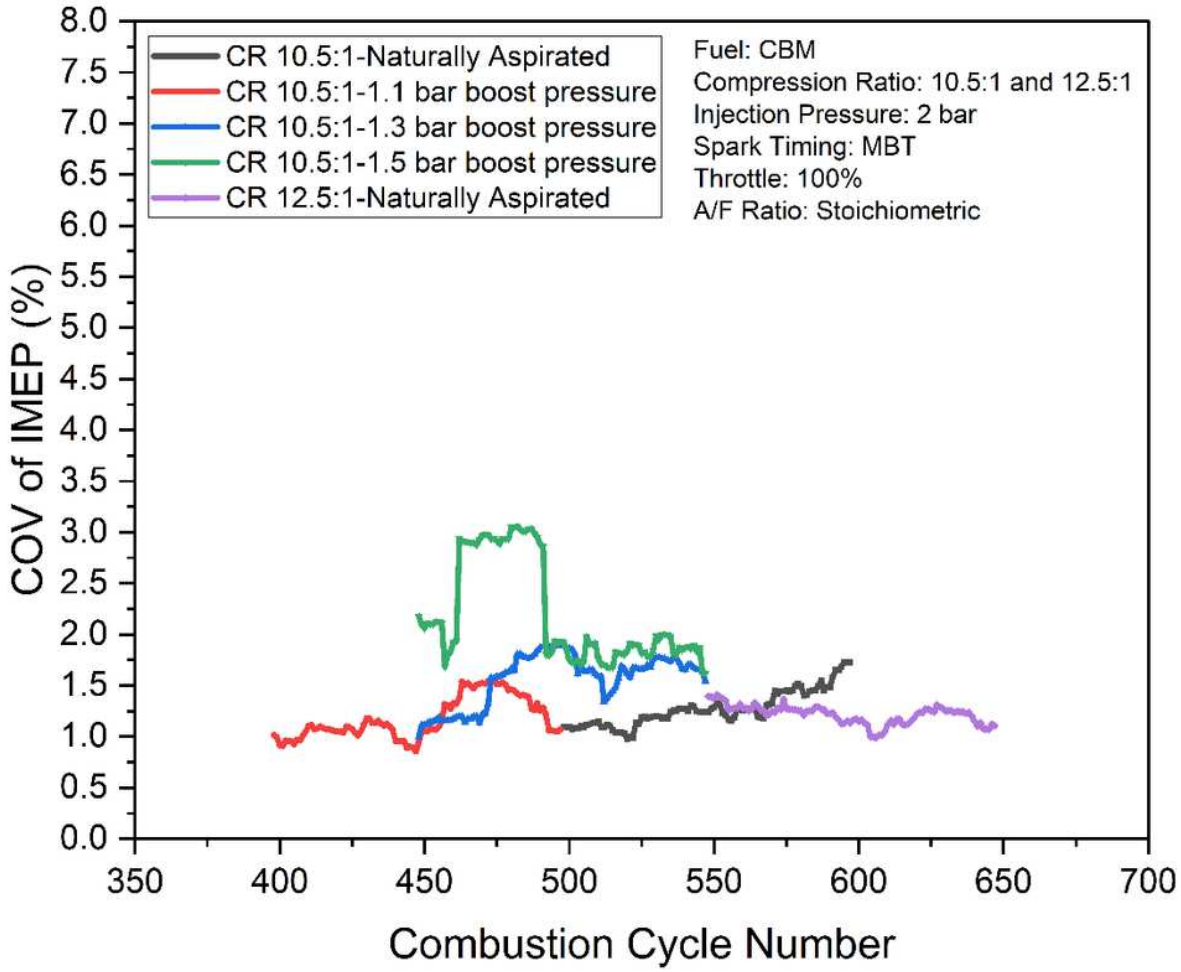

Figure 22

Variation of COV of IMEP with combustion cycle number.

Supplementary Files

This is a list of supplementary files associated with this preprint. Click to download.

- GraphicalAbstract.jpg